CZECH TECHNICAL UNIVERSITY OF PRAGUE
FACULTY OF MECHANICAL ENGINEERING

Department of Technical Mathematics

Numerical Simulation of Incompressible Flows with Variable Viscosity

author : Luboš Pirkl
supervisor : Mgr. Ing. Tomáš Bodnár PhD.

Prague, June 14, 2007

Summary

This work deals with problems of Computational Fluid Dynamics (CFD). It deals with mathematical and numerical modelling incompressible fluid flow with variable viscosity.

We started from basic physical equations describing the flow of viscous incompressible fluid. We made mathematical model and then worked out numerical simulation.

The phenomenon of variable viscosity in this work is represented by two different types of flow.

Part of this work deals with analysis and modelling of non-Newtonian fluids. Here, we concentrate on a subclass of non-Newtonian models which are often referred as generalized Newtonian models. There are a number of models of non-Newtonian viscosity presented in this work. We also made comparison of these models as well as comparison of Newtonian and non-Newtonian types of flow. Then we focused on the blood flow, as one of the most important representatives of non-Newtonian fluids.

Other part of this work deals with laminar and then turbulent flow and its modelling with help of statistical attitude to turbulence (solving RANS). From the mathematical point of view, with using Boussinesq hypothesis, the viscosity locally increases when statistical attitude to turbulence is applied. Here, we focused on basic turbulence models, algebraic model (Baldwin-Lomax) and one-equational model (Spalart-Allmaras).

We introduced and then realized two numerical methods based on Finite Volume Method. In application part of this work there are some typical test cases on which are presented and discussed the results. The test cases were chosen to be aimed on the internal aerodynamics.

Souhrn

Tato práce je zameřená na řesení problémů dynamiky tekutin. Zabýváme se v ní matematickým a numerickým modelováním nestlačitelného proudění s proměnnou viskozitou.

Postupně jsme vyšli od základních fyzikálních rovnic popisujících proudění vazké nestlačitelné tekutiny, vytvořili jsme matematický model, navrhli a posléze realizovali možné způsoby rešení.

Fenomén proměnné viskozity je v práci reprezentován dvěma odlišnými druhy proudění.

Část práce se zabývá modelováním ne-Newtonských tekutin. Zde jsme se zaměřili na skupinu nazývanou zobecněné Newtonské tekutiny. Je zde rozebrána danná problematika. Bylo vybráno několik modelů ne-Newtonské viskosity a provedeno porovnání jejich výsledků. Dále bylo realizováno srovnání proudění Newtonské a ne-Newtonské tekutiny a poukázáno na rodíly mezi těmito dvěma druhy proudění. Práce sleduje proudění lidské krve, jakožto jednoho z nejdůležitějších zástupců ne-Newtonských tekutin.

Další část této práce se zabývá turbulentním prouděním a jeho modelováním pomocí statistických modelů turbulence (řešení RANS). Na řešení turbulentního, proudění podle Boussinesquovy hypotézy, může být z matematického pohledu nahlíženo také jako na proudění s proměnnou viskositou. Zde jsme se zaměřili na jednodušší modely turbulence, algebraický model (Baldwin-Lomax) a jednorovnicový model (Spalart-Allmaras).

Navrhli jsme a vyzkoušeli dvě numerické metody založené na metodě konečných objemů. V aplikační části této práce je pak na několika typických příkladech realizováno a diskutováno jejich řešení. Testovací případy byly vybrány převážně z oblasti vnitřní aerodynamiky.

Contents

List of symbols

Latin symbols

$\boldsymbol{v}$	velocity vector
$\boldsymbol{x}$	cartesian coordinate vector
t	time
x,y,z	space coordinates (components of vector $\boldsymbol{x}$)
u,v,w	velocity components (components of vector $\boldsymbol{v}$)
f	volume force
E	energy
p	pressure
T	temperature
u	internal energy
r	universal gas constant
q	heat flux
k_t	thermal diffusion coefficient
P	additional matrix
W	vector of unknowns (conservative quantities)
F,G	vectors of inviscid (convective) fluxes
R,S	vectors of viscous (diffuse) fluxes
D	diameter
Re	Reynolds number
$\bar{\mathsf{D}}$	the rate of deformation tensor
d_{ij}	components of the rate of deformation tensor $\bar{\mathsf{D}}$
a,b	general quantity
λ	real constant
u_τ	friction velocity
C	general constant
u^+	dimensionless velocity
y^+	dimensionless distance
l_{mix}	mixing length
d_w	the distance to the solid boundary
D	cell volume
A	general matrix
DW	artificial viscosity
l_m	length of the m-th face
CFL	Courant number
M,N	the numbers of grid points
c_f	friction coefficient
U	velocity
$\mathsf{C}_\#$	test case number #
Re_T	Reynolds turbulent number
R	radius

Greek symbols

τ	shear stress
η	apparent viscosity
$\dot{\gamma}$	shear rate
μ	dynamic viscosity
μ_T	turbulent dynamic eddy viscosity
ν	kinematic viscosity
ν_T	turbulent kinematic eddy viscosity
ρ	density
β	artificial compressibility coefficient
Ψ	general quantity
τ_{ij}^R	Reynolds stress tensor
κ	Karmán's constant
δ	the boundary layer thickness
Ω_{ij}	tensor of vorticity
ϵ_2,ϵ_4	artificial viscosity coefficients
ν^x	outer normal in direction x
ρ_a,ρ_b	spectral radiuses of jacobian of inviscid fluxes
$\tilde{\eta}$	dimensionless apparent viscosity coefficient
F	function

Superscripts

a^n	time level
a'	fluctuation
$\bar{a}$	mean value
$\vec{a}$	vector
a^T	transposition

Subscripts

a_x,a_y,a_z,a_t	partial derivative with respect to axis directions and time
a_w	at the wall
a_∞	asymptotic quantity
a_T	turbulent
a_i,a_j,a_k	reference directions
a_1,a_2,a_3	related to x,y,z-axis direction

Chapter 1

Introduction

Contents

1.1 The aim of the work

This work deals with problems of Computational Fluid Dynamics (CFD). This branch is dynamically developing thanks to the strong computer technology, that considerably increased its productivity during last years. Together with experiment, the CFD analysis is necessary part of each project with a bit more sophisticated technology.

The work itself deals with numerical simulation of the incompressible fluid flow with variable viscosity. The phenomenon of variable viscosity is in this work represented by two different types of flow.

The first type of flow is flow of the non-Newtonian fluid, where the viscosity changes with the velocity field. More precisely said, with the rate of deformation tensor. Here, we concentrate on a subclass of non-Newtonian models which are often referred as generalized Newtonian models. For computation of non-Newtonian viscosity a number of models is presented. Here, we focused on the flow of human blood, as it is one of the most important representatives among non-Newtonian fluids. All the test cases of non-Newtonian flows are set to simulate human blood behavior. Flow of blood in a human body is mostly laminar, so the laminar model with non-Newtonian viscosity was used.

In the second part, changing viscosity is represented by turbulent flow. As a result of the Boussinesq hypothesis, from the mathematical point of view the viscosity locally increases when statistical attitude to turbulence is applied. Here, we presented two models of turbulence. The first one is algebraic model of turbulence, where the eddy viscosity is computed from simple algebraic relations using flow and geometry conditions. The second one is more complicated model of turbulence, where the eddy viscosity is computed with the help of another transport equation added to governing system.

We introduced and then applied two numerical methods based on Finite Volume Method. The first method, we presented is MacCormack scheme with Von Neumann - Richtmayer artificial viscosity. The second method, we presented is Causon's Modified TVD MacCormack scheme. Both methods differs only in construction of artificial viscosity. We also made comparison of accuracy of this methods.

In order to keep consistency in the scope of the work, we decided the work to be focused on internal aerodynamics. It means that we have been exploring the flow in various 2D channels and ducts. There was one exception made, that is the flat plate, falling to outer aerodynamics as one of the most common test geometries in CFD. Anyway, from computational point of view, the difference between internal and external aerodynamics is only a question of boundary conditions.

1.2 Structure of the work

The work is divided into eight chapters:

1. In *Introduction* we would like to introduce the scope of the work, determine the area of the interest of the work and present the structure of the work.
2. In the chapter called *Physical model* we want to show physical properties of the problem and make clear some terms necessary needed in following steps.
3. The chapter *Modelling Generalized Navier-Stokes equations* should introduce the problem of non-Newtonian fluids' behavior. Here, we also determine the non-Newtonian viscosity computation and mention the blood properties, as it is one of the most important representatives among non-Newtonian fluids.
4. *Turbulency modelling* is the chapter where we want to introduce basic terms of turbulence and show how it is possible to solve turbulent problem. There are presented two turbulence models, algebraic model (Baldwin-Lomax) and one-equational model (Spalart-Allmaras). In the short section the turbulent boundary is layer is shown.
5. The chapter *Mathematical model* presents the type of methods used for numerical solution.
6. In the chapter *Numerical method* we introduce the numerical methods that was used to solve test cases.
7. In the chapter *Application* there are presented typical test cases as well as numerical results. All the test cases are marked by $\mathsf{C}_{\#}$.
8. The chapter *Conclusion & Remarks* summarizes the results and closes the work.

1.3 Some preliminary ideas & simplifications

The usual way how to describe a fluid flow is by means of the expression for the flow velocity $\boldsymbol{v}$ at any point $\boldsymbol{x}$ at any time t:

$$\boldsymbol{v} = \boldsymbol{v}(\boldsymbol{x}, t) \tag{1.1}$$

The velocity field provides the information what all elements of the fluid are "doing" at given time. Finding equation (1.1) is usually the main task. In general the equation (1.1) is convenient shortcut for:

$$\boldsymbol{v} = (u, v, w)^T, \quad \boldsymbol{x} = [x, y, z] \tag{1.2}$$

and:

$$u = u(x, y, z, t), \quad v = v(x, y, z, t), \quad w = w(x, y, z, t). \tag{1.3}$$

Generally, we must expect this task to be quite difficult. In this work we did some following simplifications:

- *Incompressibility* of fluid:

$$div\, \boldsymbol{v} = 0, \tag{1.4}$$

  As incompressible fluids are commonly considered liquids. As incompressible fluids are as well considered gasses in which the density varies up to 5%, that corresponds to speeds up to ≈ 100 m/s in the atmosphere.

- *Two-dimensional* (2D) flow:

$$\boldsymbol{v} = (u(x, y, t), v(x, y, t), 0)^T, \tag{1.5}$$

  in this case velocity $\boldsymbol{v}$ is independent on one spatial coordinate (often selected to be z) and has no component in that direction.

- *Steady* flow:

$$\frac{\partial \boldsymbol{v}}{\partial t} = 0 \tag{1.6}$$

  in this case $\boldsymbol{v}$ depends on $\boldsymbol{x}$ only. At any fixed point in space speed and direction of flow are both constant.

- *Isothermal* flow:
  temperature is considered to be constant in space and time.

- *Volume forces:*
  (Coriolis force, gravity, ...) are considered to be zero.

As a result, two-dimensional steady flow is considered of the form:

$$\boldsymbol{v} = (u(x, y), (x, y), 0)^T \tag{1.7}$$

These are idealizations. No real flow can be exactly two-dimensional. On the other hand for real 3D flow we might reasonably expect a close approximation to 2D flow, assuming symmetrical or simple geometries. As well as extending 2D problem to 3D problem is possible, there are methods for unsteady flows solution, but it is not the aim of this work.

Chapter 2

Physical model

Contents

2.1 Rheological constitutive relations

Let us take closer look at some terms, which are necessary needed to be clear for better orientation in this work. Here we will describe basic information, specific details will be discussed in following chapters, if needed.

2.1.1 Shear stress

Isaac Newton was the first to express the basic law of rheology describing the flow behavior of an ideal fluid:

$$\tau = \eta\dot{\gamma} \quad [Pa] \tag{2.1}$$

where τ is shear stress in fluid, η is apparent viscosity of fluid and $\dot{\gamma}$ is shear rate. Apparent viscosity coefficient η needn't be a constant as will be shown in this work.

For simple *shear rate* rules:

$$\dot{\gamma} = \frac{du}{dy} \quad [s^{-1}] \tag{2.2}$$

2.1.2 Viscosity

Viscosity could be interpreted as a tendency of a fluid to resist to flow as a result of internal friction. There are two often used types of viscosity.

dynamic viscosity is given by:

$$\mu = \frac{\tau}{\dot{\gamma}} \quad [Pa.s] = [kg.m^{-1}.s^{-1}] \tag{2.3}$$

kinematic viscosity is given by:

$$\nu = \frac{\mu}{\rho} \quad [m^2.s^{-1}] \tag{2.4}$$

Here is an example of same typical materials' dynamic viscosity:

Substance ≈	μ [mPa.s]
Air	10^{-2}
Petrol	0.65
Water	1.0
Mercury	1.5
Grape juice	$2.0 \div 5.0$
Blood [at 37^oC]	$4.0 \div 25.0$
Olive oil	10^2
Honey	10^4
Bitumen	10^8
Glass	10^{23}

It is often considered to be constant, but in general it is function[1] of at least six parameters.

$$\eta = F\left(S, T, \dot{\gamma}, p, t, E\right) \tag{2.5}$$

- S- denotes the *physical-chemical nature* of a substance being the primary influence on viscosity.
- T- is linked to the *temperature* of substance. Experience shows that viscosity is heavily influenced by changes of temperature. In general holds for liquids: the viscosity decreases when temperature increases, and for gasses: the viscosity increases when temperature increases.
- $\dot{\gamma}$- *shear rate* is important factor influencing viscosity of many fluids, the viscosity can either decrease or increase with shear rate, this dependency will be discussed in chapter 3.
- p- *pressure* is not experienced as often as previous parameters. Pressure compresses fluids and increases intermolecular resistance. Viscosity can increase.
- t- *time* denotes the phenomenon that the viscosity of some substances, usually dispersions, depends on previous shear history.
- E - parameter *electrical field* is related to a family of suspensions characterized by the phenomenon that their flow behavior is strongly influenced by the magnitude of electrical field acting upon them. These suspensions are called "electro-viscous fluids".

[1] Schramm [14]

2.2 Balance equations in fluid dynamics

In this section[2] we will take a closer look to basic differential equations of fluid dynamics. The flow of a viscous fluid is governed by conservation of mass (continuity equation), conservation of momentum (Navier-Stokes equation), conservation of energy (energy equation). The system of equations is closed by the state equation and thermodynamic relations.

2.2.1 Continuity equation

The conservation of mass can be expressed in a differential form[3]:

$$\frac{\partial \rho}{\partial t} + \frac{\partial(\rho v_i)}{\partial x_i} = 0 \tag{2.6}$$

which is the most common variant. For the steady ($\frac{\partial}{\partial t} = 0$), incompressible flow, the equation (2.6) reduces in :

$$\frac{\partial v_i}{\partial x_i} = 0 \tag{2.7}$$

2.2.2 Momentum equation

Momentum (ρv_i) is vector, thus its conversation has to be made in each direction of all axes. This is its differential form:

$$\rho\Big(\frac{\partial v_i}{\partial t} + v_j\frac{\partial v_i}{\partial x_j}\Big) = -\frac{\partial p}{\partial x_i} + \frac{\partial}{\partial x_i}\Big[\eta\Big(\frac{\partial v_j}{\partial x_i} + \frac{\partial v_i}{\partial x_j}\Big)\Big] + \frac{\partial}{\partial x_i}\Big(-\frac{2}{3}\eta\frac{\partial v_k}{\partial x_k}\Big) + \rho f_i \tag{2.8}$$

Where f_i are volume forces[4]. For constant viscosity $\eta = \mu$ equations can be rewritten:

$$\frac{\partial v_i}{\partial t} + v_j\frac{\partial v_i}{\partial x_j} = -\frac{1}{\rho}\frac{\partial p}{\partial x_i} + \frac{1}{3}\nu\frac{\partial}{\partial x_i}\Big(\frac{\partial v_j}{\partial x_j}\Big) + \nu\frac{\partial v_i^2}{\partial x_j \partial x_i} + f_i \tag{2.9}$$

For the incompressible fluid (2.7) holds and we obtain:

$$\frac{\partial v_i}{\partial t} + v_j\frac{\partial v_i}{\partial x_j} = -\frac{1}{\rho}\frac{\partial p}{\partial x_i} + \nu\frac{\partial^2 v_i}{\partial x_j^2} + f_i \tag{2.10}$$

2.2.3 Energy equation

Energy equation is not necessarily needed for our purposes. But we mention it to be complete. This equation describes the conservation of internal energy in fluid.

$$\rho\frac{\partial \mathsf{u}}{\partial t} + \rho v_j\frac{\partial \mathsf{u}}{\partial x_j} = -p\frac{\partial v_k}{\partial x_k} + \rho q_k - \frac{\partial q_k}{\partial x_k} + \frac{1}{2}\mu\Big(\frac{\partial v_j}{\partial x_i} + \frac{\partial v_i}{\partial x_j}\Big)^2 + \lambda\Big(\frac{\partial v_k}{\partial x_k}\Big)^2 \tag{2.11}$$

The heat flux is usually described by Fourier's law:

$$\boldsymbol{q} = -k_t \mathrm{grad} T \tag{2.12}$$

Here k_t is the thermal diffusion coefficient and T is the absolute temperature. For incompressible flow, the energy equation is decoupling and can be solve separately when needed.

[2] Following Kozel & Dvořák [1]
[3] Using Einstein summation notation
[4] e.g. Gravitation

2.2.4 Equation of state

The number of mentioned governing equations is five, but gives seven unknowns: $p, u, v, w, \rho, \mathsf{u}, T$. This is why the system has to be extended by the state equation (for ideal gas):

$$p = \rho r T \tag{2.13}$$

Where r denotes the universal gas constant. Using the state equation and the thermodynamics laws, the internal energy can be expressed by the following equation[5]:

$$\mathsf{u} = c_v T \tag{2.14}$$

2.3 System of Navier-Stokes equations

From the above equations we can obtain system of Navier-Stokes equations for incompressible, viscous fluid:

$$\begin{aligned}
\frac{\partial u}{\partial x} + \frac{\partial v}{\partial y} + \frac{\partial w}{\partial z} &= 0 \qquad (2.15)\\
\rho\Big(\frac{\partial u}{\partial t} + u\frac{\partial u}{\partial x} + v\frac{\partial u}{\partial y} + w\frac{\partial u}{\partial z}\Big) &= -\frac{\partial p}{\partial x} + \frac{\partial}{\partial x}\Big(\eta\frac{\partial u}{\partial x}\Big) + \frac{\partial}{\partial y}\Big(\eta\frac{\partial u}{\partial y}\Big) + \frac{\partial}{\partial z}\Big(\eta\frac{\partial u}{\partial z}\Big) + f_1\\
\rho\Big(\frac{\partial v}{\partial t} + u\frac{\partial v}{\partial x} + v\frac{\partial v}{\partial y} + w\frac{\partial v}{\partial z}\Big) &= -\frac{\partial p}{\partial y} + \frac{\partial}{\partial x}\Big(\eta\frac{\partial v}{\partial x}\Big) + \frac{\partial}{\partial y}\Big(\eta\frac{\partial v}{\partial y}\Big) + \frac{\partial}{\partial z}\Big(\eta\frac{\partial v}{\partial z}\Big) + f_2\\
\rho\Big(\frac{\partial w}{\partial t} + u\frac{\partial w}{\partial x} + v\frac{\partial w}{\partial y} + w\frac{\partial w}{\partial z}\Big) &= -\frac{\partial p}{\partial z} + \frac{\partial}{\partial x}\Big(\eta\frac{\partial w}{\partial x}\Big) + \frac{\partial}{\partial y}\Big(\eta\frac{\partial w}{\partial y}\Big) + \frac{\partial}{\partial z}\Big(\eta\frac{\partial w}{\partial z}\Big) + f_3
\end{aligned}$$

These equations create the complete system, we will solve in this work. For more simplicity we will consider the volume forces f_i to be equal 0.

2.4 System of Navier-Stokes equations in vector form

Starting from this section we will consider all the problems in two dimensions only. For better-arranged description, let us rewrite governing equations (2.15) in (two-dimensional) vector form:

$$P\mathsf{W}_t + \mathsf{F}_x + \mathsf{G}_y = \mathsf{R}_x + \mathsf{S}_y \tag{2.16}$$

where: W denotes the vector of unknowns (conservative quantities), F, G are the vectors of inviscid (convective) fluxes, R, S are the vectors of viscous (diffuse) fluxes, P is an additional matrix, that will be discussed.

Before using *artificial compressibility method* [6] let us consider the vectors in the above equation have the following meaning:

$$\begin{aligned}
P &= diag(0,1,1) && (2.17)\\
\mathsf{W} &= (p,u,v)^T && (2.18)\\
\mathsf{F} &= (u, u^2+p, uv)^T && (2.19)\\
\mathsf{G} &= (v, uv, v^2+p)^T && (2.20)\\
\mathsf{R} &= (0, \eta u_x, \eta v_x)^T && (2.21)\\
\mathsf{S} &= (0, \eta u_y, \eta v_y)^T. && (2.22)
\end{aligned}$$

[5] assuming ideal gas

[6] see section 5.3

2.5 System of governing equations in dimensionless form

Lets rewrite the system (2.16) into the following form[7]:

$$
\begin{aligned}
P\mathsf{W}^*_t + \mathsf{F}^*_x + \mathsf{G}^*_y &= \mathsf{R}^*_x + \mathsf{S}^*_y && (2.23)\\
P &= diag(0,1,1) && (2.24)\\
\mathsf{W}^* &= (p^*, u^*, v^*)^T && (2.25)\\
\mathsf{F}^* &= (u^*, u^{*2} + p^*, u^* v^*)^T && (2.26)\\
\mathsf{G}^* &= (v^*, u^* v^*, v^{*2} + p^*)^T && (2.27)\\
\mathsf{R}^* &= (0, \eta u^*_x, \eta v^*_x)^T && (2.28)\\
\mathsf{S}^* &= (0, \eta u^*_y, \eta v^*_y)^T. && (2.29)
\end{aligned}
$$

where (*) denotes real physical values. Equations (2.23) can be transferred to the dimensionless form by following way. Each variable will be divided by its characteristic value of the same dimension.

$$v = \frac{v^*}{v_\infty} \tag{2.30}$$

Typical characteristic values are: velocity of free-stream U_∞ and some characteristic distance,e.g. diameter of channel D_∞. All of the rest variables can be extended with using combination of them:

$$x = \frac{x^*}{D_\infty}, u = \frac{u^*}{U_\infty}, p = \frac{p^*}{U^2_\infty} \tag{2.31}$$

After having used this relations and (2.23), the system of governing equations can be written in dimensionless form. Following equations describe flow of incompressible fluid:

$$P\mathsf{W}_t + \mathsf{F}_x + \mathsf{G}_y = \mathsf{R}_x + \mathsf{S}_y \tag{2.32}$$

where:

$$
\begin{aligned}
P &= diag(0,1,1) && (2.33)\\
\mathsf{W} &= (p, u, v)^T && (2.34)\\
\mathsf{F} &= (u, u^2 + p, uv)^T && (2.35)\\
\mathsf{G} &= (v, uv, v^2 + p)^T && (2.36)\\
\mathsf{R} &= \frac{1}{Re}(0, u_x, v_x)^T && (2.37)\\
\mathsf{S} &= \frac{1}{Re}(0, u_y, v_y)^T. && (2.38)
\end{aligned}
$$

where Re is called Reynolds number.

Reynolds number is the dimensionless variable, providing information of flow regime of fluid. It is a ratio of inertial and viscous forces. Up to certain (critical) value of Re a flow is laminar and after its overrun a flow becomes turbulent. Reynolds number Re is defined:

$$Re = \frac{U_\infty D_\infty}{\nu} = \frac{U_\infty D_\infty \rho}{\mu} \tag{2.39}$$

[7] subscripts x, y, z, t denotes partial derivatives with respect to time and x, y, z coordinates

2.6 Modelling Navier-Stokes equations in laminar regimes

The flow regime is laminar (the layers of the fluid don't mix together), until the Reynolds number (2.39) reaches its critical value. The governing system (2.32) is ready to solve laminar type of flow. There are not too many real cases of laminar flows. On the other hand, solution of this flow cases provides us valuable information on fluid flow behavior. Laminar cases[8] are for example the flows through tubes or capillaries (Poiseuille flows), or the flow over flat plate, or between two parallel flat plates (Couette flows).

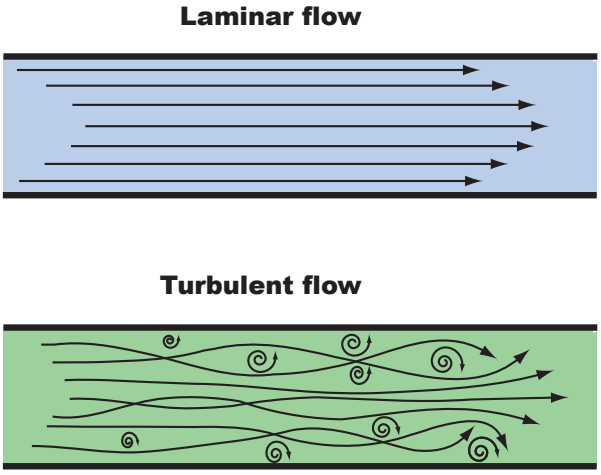

Figure 2.1: Simple illustration of the difference between laminar and turbulent flow

[8] only up to critical Reynolds number

Chapter 3

Modelling Generalized Navier-Stokes equations

Contents

3.1 Non-Newtonian fluids

3.1.1 Basic types of fluids

As we have mentioned, viscosity could be interpreted as a tendency of fluid to resist to flow as a result of internal friction. Non-Newtonian fluid is a fluid in which the viscosity changes with the shear rate due to the flow of the fluid. As a result, non-Newtonian fluids may not have a well-defined viscosity.

Although the concept of viscosity is commonly used to characterize a material, it can be inadequate to describe the mechanical behavior of a substance, particularly non-Newtonian fluids.

Let us take a closer look at the basic types of fluids behavior.

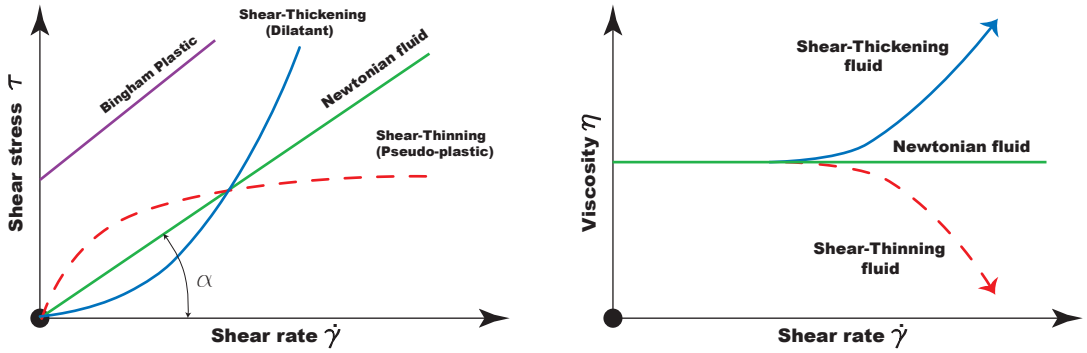

Figure 3.1: Behavior of basic types of fluids

Figure 3.1 shows[1] the behavior of basic types of fluids. For ideal fluid flow, "Newtonian fluid behavior", the graphical equivalent of shear stress is straight line, starting from the origin. The value of the shear stress can also be defined as a slope (tangent of the angle α): $\eta = \tan\alpha$. This means, that for Newtonian fluids, η is not affected by changes in the shear rate.

Bingham plastic fluid shows linear relationship between shear stress and shear rate, if once threshold shear stress is exceeded. As a Bingham plastic fluids are considered for example paste or mud.

For *shear-thickening* (dilatant) fluids the viscosity increases with shear rate. This type of behavior is not so common, As a shear-thickening fluids are considered for example sugar in water or suspension of corn starch.

The most common non-Newtonian fluid behavior in the nature is *shear-thinning* (pseudo-plastic), when the viscosity decreases with shear rate (dashed lines in figure 3.1). As a shear-thinning fluids are considered for example milk or blood.

3.1.2 Shear thinning fluid viscosity

As was written, viscosity of this group of fluids decreases when the shear rate increases. Figure 3.2 shows[2] more details of shear-thinning fluid behavior:

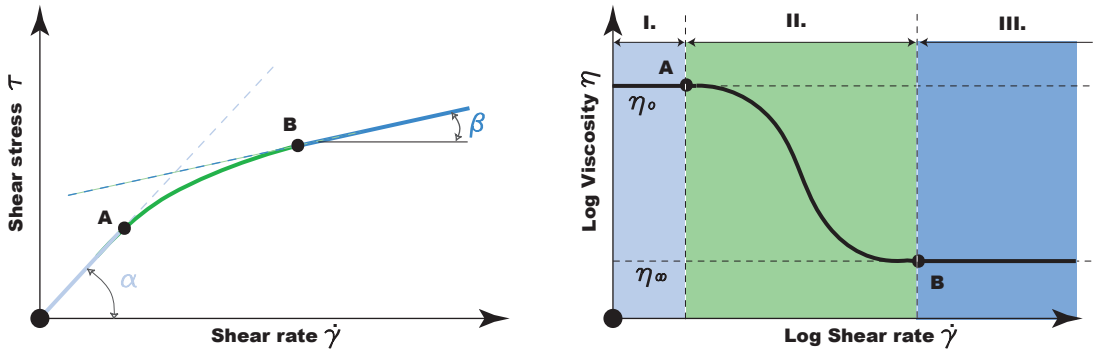

Figure 3.2: Pseudo-plastic viscosity

For low shear rates ($\eta_0 = \tan\alpha$) and for high shear rates ($\eta_\infty = \tan\beta$) the fluid shows Newtonian behavior. The problem is to catch the transition of viscosity between the points A and B, where the viscosity decreases from η_0 to η_∞. The course of viscosity can be divided into three parts. The first part ($I.$), where the viscosity η_0 is independent of shear rate and is called *zero shear viscosity*

[1] e.g. Schramm [14]
[2] Schramm [14]

is called *First Newtonian range*. In the second part ($II.$) the viscosity η drops as a result of fluid microstructure changes. This part between points A and B has to be approximated. The third part ($III.$), where the viscosity η_∞ is independent of further increasing of shear rate and is called *infinity shear viscosity* is called *Second Newtonian range*.

3.2 Viscosity of non-Newtonian fluids

3.2.1 Shear rate

For incompressible Newtonian fluids, the shear stress is proportional to the *rate of deformation tensor* $\overline{\mathsf{D}}$ (equivalent of Newton's law (2.1)) and can be expressed:

$$\tau = \mu\overline{\mathsf{D}} \tag{3.1}$$

where rate of deformation tensor $\overline{\mathsf{D}}$ is defined by :

$$\overline{\mathsf{D}} = \frac{1}{2}(\frac{\partial v_i}{\partial x_j} + \frac{\partial v_j}{\partial x_i}) \tag{3.2}$$

and μ[3] is viscosity, which is independent of $\overline{\mathsf{D}}$. For non-Newtonian fluids, the shear stress can similarly be written in terms of a non-Newtonian apparent viscosity η[4] :

$$\tau = \eta(\overline{\mathsf{D}})\overline{\mathsf{D}} \tag{3.3}$$

In general, η is a function of all three invariants of the rate of deformation tensor $\overline{\mathsf{D}}$. But for incompressible fluids, η is considered to be function of the *shear rate* $\dot{\gamma}$ only[5]. $\dot{\gamma}$ is related to the second invariant of $\overline{\mathsf{D}}$ and is defined as :

$$\dot{\gamma} = \frac{1}{2}\sqrt{\overline{\mathsf{D}} : \overline{\mathsf{D}}} = \frac{1}{2}\sqrt{\sum_{i,j} d_{i,j}^2} \tag{3.4}$$

As a result of the above assumptions apparent viscosity η is function of shear rate $\dot{\gamma}$ and shear stress can be expressed:

$$\tau = \eta(\dot{\gamma})\overline{\mathsf{D}} \tag{3.5}$$

3.2.2 Apparent viscosity function

Apparent viscosity is computed from simple algebraic model, which is determined by numerical fitting of experimental data. We have used following models[6], set for human blood:

[3] constant
[4] function of velocity field
[5] e.g. Šesták J. & Rieger F. [9]
[6] Yeleswarapu [18]

Model name	Model equation	Model coeffitients
Modified Cross	$\eta = \eta_\infty + (\eta_0 - \eta_\infty)\left[\frac{1}{[1+(\lambda\dot{\gamma})^m]^a}\right]$	η_0=0.056 Pa.s, η_∞=0.00345 Pa.s, λ = 3.736 s, m=2.406, a=0.254
Powell-Eyring	$\eta = \eta_\infty + (\eta_0 - \eta_\infty)\left[\frac{sinh^{-1}\lambda\dot{\gamma}}{\lambda\dot{\gamma}}\right]$	η_0=0.056 Pa.s, η_∞=0.00345 Pa.s, λ=5.383 s
Modified Powell-Eyring	$\eta = \eta_\infty + (\eta_0 - \eta_\infty)\left[\frac{ln(\lambda\dot{\gamma}+1)}{[\lambda\dot{\gamma}]^m}\right]$	η_0=0.056 Pa.s, η_∞=0.00345 Pa.s, λ = 2.415 s, m=1.089
Cross	$\eta = \eta_\infty + (\eta_0 - \eta_\infty)\left[\frac{1}{1+[\lambda\dot{\gamma}]^m}\right]$	η_0=0.056 Pa.s, η_∞=0.00345 Pa.s, λ = 1.007 s, m=1.028
Simplified Cross	$\eta = \eta_\infty + (\eta_0 - \eta_\infty)\left[\frac{1}{1+\lambda\dot{\gamma}}\right]$	η_0=0.13 Pa.s, η_∞=0.005 Pa.s, λ = 8.0 s
Carreau	$\eta = \eta_\infty + (\eta_0 - \eta_\infty)\left[1 + (\lambda\dot{\gamma})^2\right]^{\frac{n-1}{2}}$	η_0=0.056 Pa.s, η_∞=0.00345 Pa.s, λ = 3.313 s, n=0.3568
Carreau-Yasuda	$\eta = \eta_\infty + (\eta_0 - \eta_\infty)\left[1 + (\lambda\dot{\gamma})^a\right]^{\frac{n-1}{a}}$	η_0=0.056 Pa.s, η_∞=0.00345 Pa.s, λ =1.902 s, n=0.22,a=1.25
Power-Law	$\eta = m\dot{\gamma}^{n-1}$	η_{min}=0.00345 Pa.s, η_{max}=0.056 Pa.s, n=0.60,m=0.35

Table 3.1: Apparent viscosity models

where the model coefficients are set for human blood adopted from Cho & Kensey [17] .

3.3 Governing equations

Generalized Navier-Stokes equations for two-dimensional case can be written in following form :

$$\begin{pmatrix} 0 \\ u \\ v \end{pmatrix}_t + \begin{pmatrix} u \\ u^2+p \\ uv \end{pmatrix}_x + \begin{pmatrix} v \\ vu \\ v^2+p \end{pmatrix}_y = \begin{pmatrix} 0 \\ \tilde{\eta}u_x \\ \tilde{\eta}v_x \end{pmatrix}_x + \begin{pmatrix} 0 \\ \tilde{\eta}u_y \\ \tilde{\eta}v_y \end{pmatrix}_y \tag{3.6}$$

here $\tilde{\eta}$ denotes dimensionless apparent viscosity coefficient related to η according to (2.32).

3.4 Blood behavior

3.4.1 About blood

Blood is undeniably the most important bodily fluid. It performs the essential function of providing nutrition and gas exchange for all tissues, maintaining chemical and thermal equilibrium of the body and defending against infection trough the action of antibodies. The blood circulation in the human body depends not only on the driving force of the heart and the mechanical properties of the vascular system, but also on the rheology of blood itself.

The first known attempts to study the flow properties of blood were made by Young and Poiseuille in the seventeen century, who estimated the resistance to blood flow by means of flow experiments in tubes. Although Poiseuille knew that some deviations from others fluids exists, they considered blood to be Newtonian fluid. Later in twentieth century Denning & Watson and Fahraeus & Lindqvist observed the anomalous flow property of blood that viscosity appear to depend upon the diameter to the tube used for the measurement. The development of rotational viscometers in the middle of twentieth century facilitated rigorous experimentations towards the study of the abnormal flow properties of blood. The investigations essentially showed that the blood is shear thinning non-Newtonian fluid.

3.4.2 Microstructure of blood

Blood is a suspension of large number of formed elements (*cells*) in an aqueous polymer solution (*plasma*). There are three kinds of cells: Red blood cells (RBC) , white blood cells (WBC) and platelets. RBC has biconcave shape with diameter of about $7 \cdot 10^{-6} m$. The blood cells are present in a ratio of approximately 45% cells and 55% plasma.

Plasma contains water (approximately 90-92% by weight), mineral ions such as K^+, Na^-, Cl^-, HCO_3^-, HPO_4^-, (approximately 1-2%) and the reminder (7%) are various proteins. Following figure illustrates bloodstream and the basic members that can be find in it:

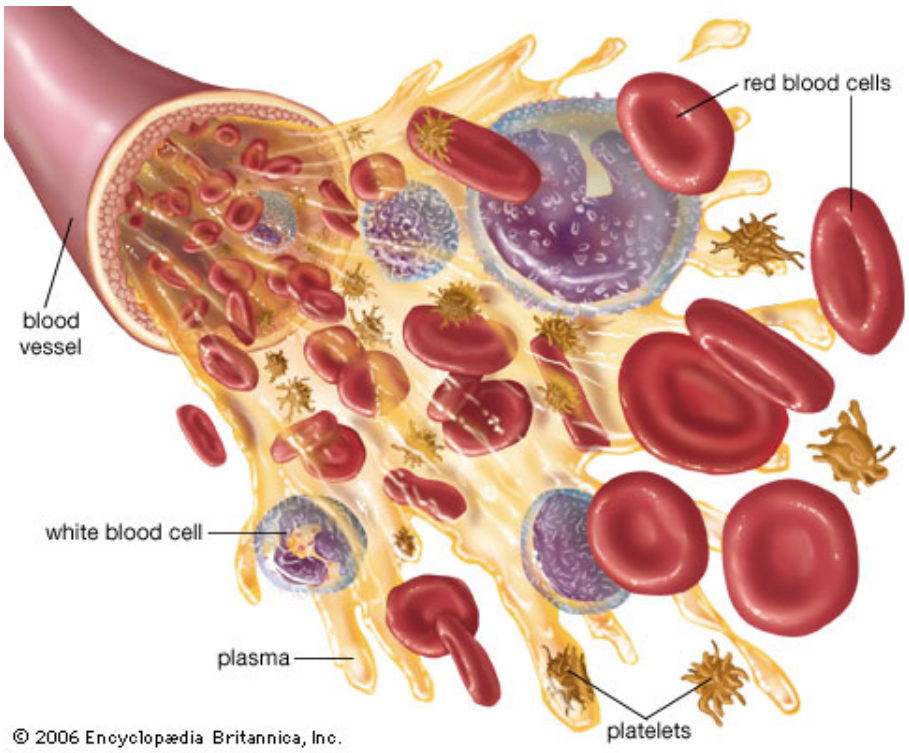

Figure 3.3: The microstructure of the blood

3.4.3 Aggregation and deformability of red blood cells

The red blood cells have a tendency to attach themselves side by side to form what are described as rouleaux, resembling a stack of coins. The phenomena to form rouleaux is called *aggregation*. The attraction is attributed to charged groups on the surface of cells. The process is reversible and also depends on the presence fibrinogen and globulins.

The red blood cells also can *deform* into a infinite variety of shapes without changing volume or surface area as is shown in following figure:

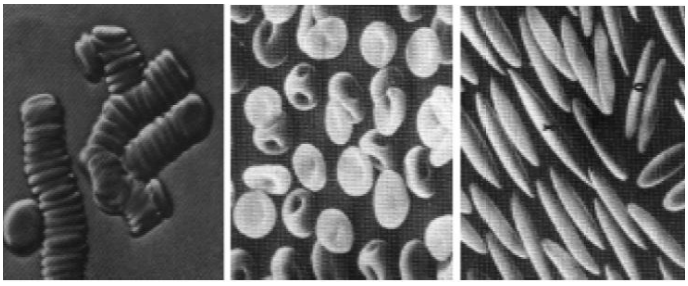

Figure 3.4: Rouleaux, normal cells and deformed cells under microscope

At high shear rates RBCs exist as an individual particles (like if layers of fluid cut rouleaux) and take a thinner shape. At lower shear rates they aggregate, forming rouleaux resulting in an increase of viscosity. Aggregation and deformability of red blood cells just cause the blood non-Newtonian behavior.

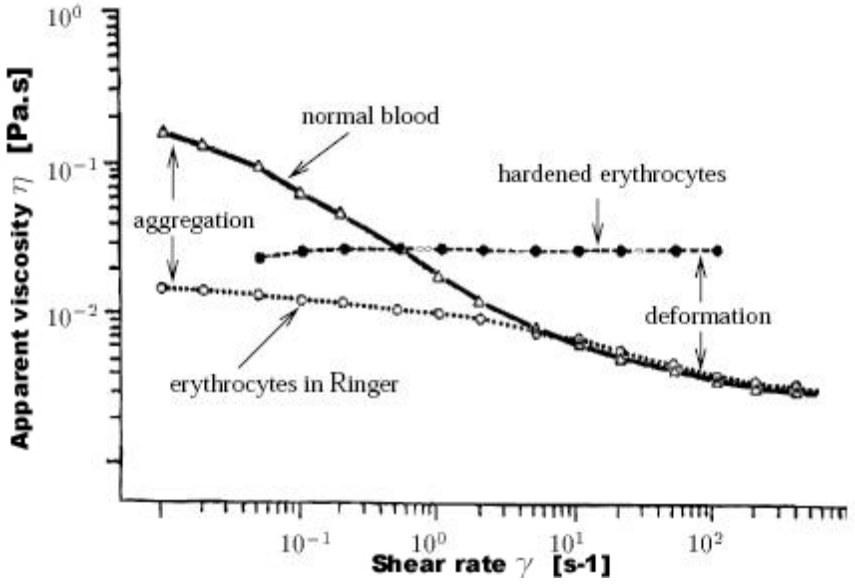

Figure 3.5: Viscosity influenced by aggregation and deformability of red blood cells

Chapter 4

Turbulence modelling

Contents

4.1 Introduction to turbulence

4.1.1 What is turbulence?

In this section[1] we will take a closer look at turbulence in general. Most fluid flows in the nature and in technical applications are turbulent. Turbulence appears in all fluids and at all speeds from low speeds in the sea or in the atmosphere to supersonic speeds in technical applications. Turbulence appears in every fluid, when inertial or volume forces in the fluid are great enough in comparison with viscous forces that damp accidental disorders or non-stabilities of flow. If critical Reynolds number overruns, laminar flow regime turns into turbulent. Turbulence is three-dimensional non-stationary motion of viscous fluid, that has four attributes:

- **Non-deterministic changes in time**
- **Turbulent transport of momentum, mass and heat**
- **Vorticity and three-dimensional character**
- **Dissipation of turbulent kinetic energy**

[1] Following Příhoda & Louda [16]

Turbulent flow consists of spectrum of turbulent whirls, whose size differs from the smallest ones, where turbulent kinetic energy dissipates in heat, to greatest ones, whose size equals to geometry of flow. Over accidental character of turbulence, the same boundary conditions lead to the same flow characteristics. Turbulence can be considered as a result of quasi-deterministic processes in flowing fluid. The mean flow of the fluid can be described with the help of statistic laws.

4.1.2 How to model turbulence?

Turbulence modelling is extremely complicated task. Solution still arises from conservation laws. It is always only some approximation because we describe the mean values only. Governing equations are system of Navier-Stokes equations. For description of turbulent flow, especially in technician applications, the mean parameters of flow are important. There are two main attitudes of numerical solution of governing equations: The first one is the direct attitude called *Direct Numerical Simulation* (DNS). DNS requires very thick mesh, especially near the walls. The number of needed vertices of the mesh is proportional to $Re^{\frac{9}{4}}$, so the requirements quickly increase with increasing of Reynolds number. These days[2] DNS can be realized on special high efficient computers only and nothing signalizes dramatic changes in near [3] future.

The second possibility is to apply statistic approach. It is based on decomposition[4] of instantaneous values of variables into mean part and fluctuation part. Then the governing system called *Reynolds Averaged Nevier-Stokes equations* (RANS) is solved for the mean values only and is completed by the turbulence model.

The compromise between DNS and RANS is *Large Eddy simulation* (LES). Here the filter of whirls is applied. The great whirls are simulated directly and small whirls are modelled by sub-grid model.

4.2 Averaging process

4.2.1 Reynolds decomposition (averaging) with respect to time

Statistic approach to turbulence is based on decomposition and time averaging of instantaneous values of variables into mean part and fluctuation part. If the mean value does not depend on choice of initial time (stationary process in mean values) the mean value can be expressed[5]:

$$\bar{\Phi}(x_i) = \lim_{\Delta t \to \infty} \frac{1}{\Delta t} \int_{t_0}^{t_0+\Delta t} \Phi(x_i, t) dt \tag{4.1}$$

After Reynolds averaging each instantaneous value can be substitute by its mean part and its fluctuation part:

$$a = \bar{a} + a' \tag{4.2}$$

The following rules will be used:

$$\begin{aligned} \bar{a'} &= 0 && (4.3)\\ \overline{ab} &= \overline{ab} + \overline{a'b'} && (4.4)\\ \overline{a+b} &= \bar{a} + \bar{b} && (4.5)\\ \overline{\alpha a} &= \alpha \bar{a} && (4.6)\\ & && (4.7) \end{aligned}$$

Here a,b denotes the turbulent quantities and α is real constant.

[2] 03 2007
[3] tens of years ?
[4] Reynolds,1885
[5] e.g. Příhoda & Louda [16]

Now, let us write the velocity components and pressure in incompressible two dimensional Navier-Stokes equations (2.32) in the following form:

$$u = \bar{u} + u' \tag{4.8}$$
$$v = \bar{v} + v' \tag{4.9}$$
$$p = \bar{p} + p' \tag{4.10}$$
$$\tag{4.11}$$

Substituting these relations in the system of Navier-Stokes equations we obtain the system of Reynolds Averaged Navier-Stokes equations:

$$\frac{\partial \bar{v}_i}{\partial x_i} = 0 \tag{4.12}$$
$$\frac{\partial \bar{v}_j}{\partial t} + \bar{v}_i \frac{\partial \bar{v}_j}{\partial x_i} = -\frac{1}{\rho}\frac{\partial \bar{p}}{\partial x_i} + \frac{\partial}{\partial x_i}\Big(\nu \frac{\partial \bar{v}_i}{\partial x_j} + \tau_{ij}^R\Big) \tag{4.13}$$

where:

$$\tau_{ij}^R = -\overline{v_i' v_j'} \tag{4.14}$$

are components of the so-called *Reynolds stress tensor*. One can see, that this system differs from the original one, just in the term τ_{ij}^R. The tensor τ_{ij}^R represents six[6] (because of symmetry) additional unknowns in our new governing system. Thus, we need to complete the system by some more relations for components of Reynolds stress tensor. This problem is so-called *closure problem*.

4.2.2 The closure problem

As it was written, the basic problem of solving RANS is in approximating Reynolds stress tensor. System cannot be closed directly by equations for Reynolds stresses because equations contain unknown correlations of fluctuations of velocity and pressure. For closing the system of equations we have to approximate the Reynolds stress tensor (models of the first order) or approximate unknowns in transport equations for Reynolds stresses (models of the second order).

In 19. century *Boussinesq* formed hypothesis that exists some analogy between molecular and turbulent viscosity. He claimed that analogically to the Newton's law (2.1), it is possible to express turbulent stress in similar way like shear stress. Using this hypothesis, we can introduce the *turbulent eddy viscosity* ν_T and Reynolds stress tensor can be written in the following way:

$$\tau_{ij}^R = -\overline{v_i' v_j'} \approx \nu_T\Big(\frac{\partial \bar{v}_i}{\partial x_j} + \frac{\partial \bar{v}_j}{\partial x_i}\Big) \tag{4.15}$$

This turbulent viscosity hypothesis comes from idea of similarity of molecular transport of momentum with turbulent transport, which is supported by whirls much more greater than are sizes of molecules. Over great differences between these processes Boussinesq hypothesis gives satisfying results.

Introduction of turbulent eddy viscosity does not solve the closure problem. It is only substitution of the Reynolds stress tensor[7] by turbulent eddy viscosity[8].

It is necessary to use some turbulence model to evaluate turbulent eddy viscosity. Here we will just mention some basic categorization of RANS models:

- Algebraic models
- One-equation models
- Two-equation models

} first order models

- Reynolds stress models } second order models

[6] in three dimensions
[7] tensor of second order
[8] scalar

This work is aimed on algebraic and one-equational models.

4.3 Turbulent boundary layer

The turbulent flow near solid boundaries is described by empirically-determined relationships called *the law of the wall*. Measurements show, that for turbulent flows, the velocity near the wall varies logarithmically with the distance from the surface. From dimensional analysis[9] we obtain the law of the wall:

$$\frac{u}{u_\tau} = \frac{1}{\kappa} ln \frac{u_\tau y}{\nu} + C \tag{4.16}$$

where κ is *Kármán's constant* and the quantity u_τ is known as the *friction velocity*:

$$u_\tau = \sqrt{\frac{\tau_w}{\rho}} \tag{4.17}$$

Correlation of measurements indicate $C \approx 5.0$ and $\kappa \approx 0.41$.

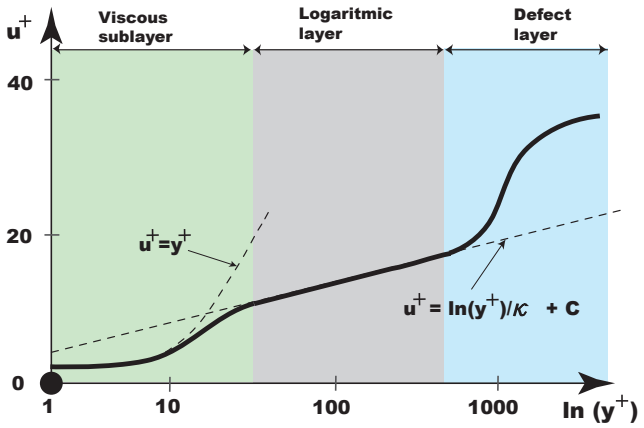

Figure 4.1: Typical velocity profile for a turbulent boundary layer

Figure (4.1) shows typical velocity profile for a turbulent boundary layer. The graph displays the dimensionless velocity u^+, and dimensionless distance y^+, defined as:

$$u^+ = \frac{U}{u_\tau}, \quad y^+ = \frac{u_\tau y}{\nu}. \tag{4.18}$$

The velocity profile matches the law of the wall for values of y^+ in excess of about 30.

4.4 Algebraic turbulence models

Algebraic models (zero-equation models) are the simplest turbulence models. These models use the Boussinesq eddy viscosity approximation to compute the Reynolds stress tensor as the product of an eddy viscosity and the mean strain-rate tensor. In contrast to the molecular viscosity, which is an intrinsic property of the fluid, the eddy viscosity depends on the flow. Most of them rely on *Prandtl's mixing length hypothesis* and are specified by an algebraic relation between eddy viscosity and length scales of the mean flow. Thus, algebraic models are, by definition, incomplete models of turbulence. Although, they have proven to be useful in many engineering fields.

[9] e.g. Wilcox [3]

4.4.1 Prandtl's mixing length hypothesis

In 1925 Prandtl visualized a simplified model for turbulence motion and expressed idea of mixing length, to be distance which is travelled by the turbulent whirl before is destroyed by mixing. Prandtl's mixing length hypothesis leads to formula for dynamic eddy viscosity:

$$\mu_T = \rho l_{mix}^2 \left| \frac{\partial u}{\partial y} \right| \tag{4.19}$$

where l_{mix} is mixing length. Prandtl postulated further for flows near solid boundaries the mixing length is proportional to distance from the surface:

$$\frac{l_{mix}}{\delta} = F\left(\frac{d_w}{\delta}\right) \tag{4.20}$$

where d_w is the distance to nearest wall and δ is boundary layer thickness, which is distance for which holds:

$$\frac{\boldsymbol{v}}{\boldsymbol{v}_\infty} = 0.99 \tag{4.21}$$

4.5 Baldwin - Lomax algebraic model

The Baldwin-Lomax model (Baldwin and Lomax (1978), [21]) is a two-layer algebraic which gives the eddy viscosity ν_T as a function of the local boundary layer velocity profile. The model is suitable for high-speed flows with thin attached boundary-layers, typically present in aerospace and turbomachinery applications. It is commonly used in quick design iterations where robustness is more important than capturing all details of the flow physics. The Baldwin-Lomax model is not suitable for cases with large separated regions and significant curvature/rotation effects.

$$\nu_T = \begin{cases} \nu_{Tinner} \ \ldots \text{ if } y \leq y_{crossover} \\ \nu_{Touter} \ \ldots \text{ if } y > y_{crossover} \end{cases} \tag{4.22}$$

where $y_{crossover}$ is the smallest distance from the surface where ν_{Tinner} is equal to ν_{Touter}:

$$y_{crossover} = MIN(y): \ \nu_{Tinner} = \nu_{Touter} \tag{4.23}$$

The inner region is given by Prandtl - Van Driest formula:

$$\boxed{\nu_{Tinner} = l_{mix}^2 \, |\Omega|} \tag{4.24}$$

where:

$$l_{mix} = \kappa y \left(1 - e^{\frac{-y^+}{A^+}}\right) \tag{4.25}$$

and

$$y^+ = \frac{\rho_w v_\tau d_w}{\mu_w} = \frac{\sqrt{\rho_w \tau_w} d_w}{\mu_w} \tag{4.26}$$

and

$$\Omega_{ij} = \frac{1}{2}\left(\frac{\partial v_i}{\partial x_j} - \frac{\partial v_j}{\partial x_i}\right), |\Omega| = \sqrt{2\Omega_{ij}\Omega_{ij}} \tag{4.27}$$

The outer region is given by:

$$\boxed{\nu_{Touter} = \rho \, K \, C_{CP} \, F_{WAKE} \, F_{KLEB}(y)} \tag{4.28}$$

where:

$$F_{WAKE} = MIN\left(y_{MAX}\, F_{MAX}\ ;\ C_{WK}\, y_{MAX}\, \frac{u_{DIF}^2}{F_{MAX}}\right) \tag{4.29}$$

where y_{MAX} and F_{MAX} are determined from the maximum of the function:

$$F(y) = y\,|\Omega|\left(1 - e^{\frac{-y^+}{A^+}}\right) \tag{4.30}$$

where F_{KLEB} is the intermittency factor given by:

$$F_{KLEB}(y) = \left[1 + 5.5\left(\frac{y\, C_{KLEB}}{y_{MAX}}\right)^6\right]^{-1} \tag{4.31}$$

u_{DIF} is the difference between maximum and minimum speed in the profile. For boundary layers the minimum is always set to zero.

$$u_{DIF} = MAX(\sqrt{u_i u_i}) - MIN(\sqrt{u_i u_i}) \tag{4.32}$$

The table below gives the model constants present in the formulas above.

A^+	C_{CP}	C_{KLEB}	C_{WK}	κ	K
26.0	1.6	0.3	0.25	0.41	0.0168

4.5.1 System of governing equations including Baldwin-Lomax model

When using algebraic turbulence model, the system of governing equations can be rewritten in the following form:

$$\begin{pmatrix} 0 \\ u \\ v \end{pmatrix}_t + \begin{pmatrix} u \\ u^2 + p \\ uv \end{pmatrix}_x + \begin{pmatrix} v \\ vu \\ v^2 + p \end{pmatrix}_y = \begin{pmatrix} 0 \\ (\nu + \nu_T)u_x \\ (\nu + \nu_T)v_x \end{pmatrix}_x + \begin{pmatrix} 0 \\ (\nu + \nu_T)u_y \\ (\nu + \nu_T)v_y \end{pmatrix}_y \tag{4.33}$$

4.5.2 Performance, applicability and limitations of the Baldwin-Lomax model

The Baldwin-Lomax model[10] is suitable for high-speed flows with thin attached boundary layers. Typical applications are aerospace and turbomachinery applications. It is a low-Re model and as such it requires a fairly well-resolved grid near the walls, with the first cell located at $y^+ < 1$.

The model is popular in quick design-iterations due to its robustness and reliability. It seldom leads to any convergence problems and it seldom gives completely unphysical results.

The computation of most of the model looks to relatively straightforward. The model is nonlocal in nature due to the presence of the damping function. This means that for any location in the flow interior, we need a wall (or other suitable location) to compute a y^+ from. Further, the calculation of y_{MAX} and F_{MAX} is better suited to a structured grid in which grid lines emanate outward from a wall (or wakeline, etc.).

The determination of y_{MAX} and F_{MAX} is sensitive to gridpoint location, as the vorticity magnitude is typically only available pointwise. Finally, it is tempting to use the minimum of the two (inner and outer) eddy viscosity results (as well in our case) instead of the correct crossover formula. This simplifies the programming, but is not justifiable on any other grounds (and can lead to the use of the wrong eddy viscosity). The (minimal) additional programming is required for correct implementation of this model.

[10] Following [32]

4.6 Spalart - Allmaras model

Spalart-Allmaras model (SA) presented by Spalart and Allmaras [24] is an one-equational model written in terms of modified eddy viscosity. The model uses empiricism and arguments of dimensional analysis, it is independent on y^+, but requires the distance to the nearest wall d_w. The turbulent eddy viscosity is developed with the help of model's transport equation:

$$\frac{\partial\tilde{\nu}}{\partial t}+u_j\frac{\partial\tilde{\nu}}{\partial x_j}=\underbrace{C_{b1}[1-f_{t2}]\tilde{S}\tilde{\nu}}_{\text{production term}}+\underbrace{\frac{1}{\sigma}\{\frac{\partial}{\partial x_j}[(\nu+\tilde{\nu})\frac{\partial\tilde{\nu}}{\partial x_j}]+C_{b2}\frac{\partial\tilde{\nu}}{\partial x_j}\frac{\partial\tilde{\nu}}{\partial x_j}\}}_{\text{diffusion term}}-\underbrace{\left[C_{w1}f_w-\frac{C_{b1}}{\kappa^2}f_{t2}\right]\left(\frac{\tilde{\nu}}{d}\right)^2}_{\text{destruction term}}+f_{t1}\Delta U^2 \tag{4.34}$$

where the production term is developed with the help of norm of vorticity $|\Omega|$. The diffusion terms are naturally connected with spatial derivatives of $\tilde{\nu}$. The destruction term arose from dimensional analysis. f_{t1} and f_{t2} are transition functions, that provide control over the laminar and turbulent regions. All the details are step by step discussed in the original article [24]. The turbulent eddy viscosity is then:

$$\nu_T=\tilde{\nu}f_{v1},\quad f_{v1}=\frac{\chi^3}{\chi^3+C_{v1}^3},\quad \chi=\frac{\tilde{\nu}}{\nu} \tag{4.35}$$

where $\chi=Re_T$ is Reynolds turbulent number. Model is completed by following formulas:

$$\tilde{S}\equiv|\Omega|+\frac{\tilde{\nu}}{\kappa^2d^2}f_{v2},\quad f_{v2}=1-\frac{\chi}{1+\chi f_{v1}} \tag{4.36}$$

$$f_w=g\left[\frac{1+C_{w3}^6}{g^6+C_{w3}^6}\right]^{1/6},\quad g=r+C_{w2}(r^6-r),\quad r\equiv\frac{\tilde{\nu}}{\tilde{S}\kappa^2d^2} \tag{4.37}$$

$$f_{t1}=C_{t1}g_t\exp\left(-C_{t2}\frac{\omega_t^2}{\Delta U^2}[d^2+g_t^2d_t^2]\right) \tag{4.38}$$

$$f_{t2}=C_{t3}\exp(-C_{t4}\chi^2) \tag{4.39}$$

The following table gives the model constants present in the formulas above:

σ	C_{b1}	C_{b2}	κ	C_{w1}	C_{w2}	C_{w3}	C_{v1}	C_{t1}	C_{t2}	C_{t3}	C_{t4}
$\frac{2}{3}$	0.1355	0.622	0.41	$C_{b1}/\kappa^2+(1+C_{b2})/\sigma$	0.3	2.0	7.1	1.0	2.0	1.1	2.0

4.6.1 Finite volume method applied on Spalart-Allmaras model

We decided to use the Spalart-Allmaras model without transition corrections ($f_{t1}=f_{t2}=0$). Finite volume method (5.1) can be applied on Spalart-Allmaras transport equation by the analogical way:

$$\int_V\Big[\frac{\partial\tilde{\nu}}{\partial t}\Big]dA=-\oint_{\partial V}\Big[\tilde{\nu}v\Big]d\vec{n}+\frac{1}{\sigma}\oint_{\partial V}\Big[(\nu+\tilde{\nu})\frac{\partial\tilde{\nu}}{\partial x_j}\Big]d\vec{n}+\int_V\Big[C_{b1}\tilde{S}\tilde{\nu}+\frac{1}{\sigma}C_{b2}\frac{\partial\tilde{\nu}}{\partial x_j}\frac{\partial\tilde{\nu}}{\partial x_j}-C_{w1}f_w\Big(\frac{\tilde{\nu}}{d_w}\Big)^2\Big]dA \tag{4.40}$$

$$\frac{\partial\tilde{\nu}}{\partial t}=-\frac{1}{\mathsf{D}}\oint_{\partial V}\Big[\tilde{\nu}v\Big]d\vec{n}+\frac{1}{\sigma\mathsf{D}}\oint_{\partial V}\Big[(\nu+\tilde{\nu})\frac{\partial\tilde{\nu}}{\partial x_j}\Big]d\vec{n}+C_{b1}\tilde{S}\tilde{\nu}+\frac{1}{\sigma}C_{b2}\frac{\partial\tilde{\nu}}{\partial x_j}\frac{\partial\tilde{\nu}}{\partial x_j}-C_{w1}f_w\Big(\frac{\tilde{\nu}}{d_w}\Big)^2 \tag{4.41}$$

4.6.2 System of governing equations including Spalart-Allmaras model

The system of governing equations was simply completed by one differential (transport) equation supporting eddy viscosity. The system can be rewritten in the following form:

$$\begin{pmatrix} 0 \\ u \\ v \\ \tilde{\nu} \end{pmatrix}_t + \begin{pmatrix} u \\ u^2+p \\ uv \\ u\tilde{\nu} \end{pmatrix}_x + \begin{pmatrix} v \\ vu \\ v^2+p \\ v\tilde{\nu} \end{pmatrix}_y = \begin{pmatrix} 0 \\ (\nu+\nu_T)u_x \\ (\nu+\nu_T)v_x \\ \frac{\nu+\tilde{\nu}}{\sigma}\tilde{\nu}_x \end{pmatrix}_x + \begin{pmatrix} 0 \\ (\nu+\nu_T)u_y \\ (\nu+\nu_T)v_y \\ \frac{\nu+\tilde{\nu}}{\sigma}\tilde{\nu}_y \end{pmatrix}_y + Q \quad (4.42)$$

where the source member Q has following meaning:

$$Q = \begin{pmatrix} 0 \\ 0 \\ 0 \\ C_{b1}\tilde{S}\tilde{\nu} + \frac{1}{\sigma}C_{b2}\frac{\partial\tilde{\nu}}{\partial x_j}\frac{\partial\tilde{\nu}}{\partial x_j} - C_{w1}f_w\left(\frac{\tilde{\nu}}{d_w}\right)^2 \end{pmatrix} \quad (4.43)$$

4.6.3 Model's initial and boundary conditions

Initial and boundary conditions for p, u, v are the same as in other cases. For the "new" conservative quantity $\tilde{\nu}$ we have used following conditions:

- **Initial condition:** $\tilde{\nu} = 0.1\nu$
- **Inlet:** $\tilde{\nu} = 0.0$
- **Outlet:** $\frac{\partial\tilde{\nu}}{\partial\vec{n}} = 0.0$
- **Walls:** $\tilde{\nu} = 0.0$

4.6.4 Performance, applicability and limitations of the Spalart-Allmaras model

The wall and freestream boundary conditions are trivial $\tilde{\nu} = 0$. This is why the model is not sensitive on ν_T outer part of the boundary layer. The behavior of ν_T near the wall is almost linear, thus the solution of equation (4.34) does not require thicker mesh than the algebraic model. The model can be used for compressible flows or unstructured grids. Spalart and Allmaras tested the model as well as on boundary layer equations as on RANS. The model was tested and calibrated on RAE 2822 airfoil and in general gives better results than Baldwin-Lomax model.

Chapter 5

Mathematical model

Contents

5.1 Finite volume method

Finite volume method[1] (FVM) is developed for cases of general (nonorthogonal) meshes. Let us consider the closed area Γ with finite number of disjoint cells $\mathsf{D}_{i,j}$. Figure 5.1 shows two most common types of meshes for FVM. The first one is made of triangles and the second one is made of quadrilaterals. The advantage of the first one (so-called: unstructured triangular mesh) is to be easier generated for difficult types of geometry of the areas and also possibility of local refinement of the mesh. On the other hand the structured mesh consisting of quadrilateral cells allows very efficient saving data to two-dimensional fields and it is possible to easily implement a number of numerical methods. For example **MacCormack** scheme which was used in our case.

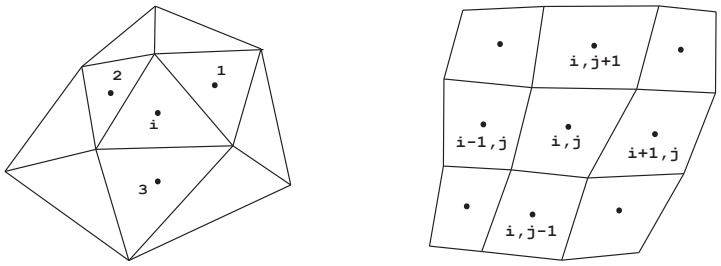

(a) Unstructured mesh (b) Structured mesh

Figure 5.1: Types of meshes

5.2 Finite volume discretization

In all our tested problems we used non-orthogonal quadrilateral mesh. Let us rewrite the equation (2.32) in another form[2]:

[1] e.g. [8]
[2] Bodnár [2]

$$\mathsf{W}_t + (\mathsf{F} - \mathsf{R})_x + (\mathsf{G} - \mathsf{S})_y = 0 \tag{5.1}$$

After its space integration we get:

$$\int_{\mathsf{D}_{i,j}} \mathsf{W}_t dS + \int_{\mathsf{D}_{i,j}} \Big[(\mathsf{F} - \mathsf{R})_x + (\mathsf{G} - \mathsf{S})_y\Big] dS = 0 \tag{5.2}$$

After application **Green's theorem** we get:

$$\int_{\mathsf{D}_{i,j}} \mathsf{W}_t dS + \oint_{\partial \mathsf{D}} \big[(\mathsf{F} - \mathsf{R})dy + (\mathsf{G} - \mathsf{S})dx\big] = 0 \tag{5.3}$$

Now we can replace, $\mathsf{W}_{i,j} = \frac{1}{|\mathsf{D}|}\int_{\mathsf{D}} \mathsf{W} dS$, the cell average of W over the cell $\mathsf{D}_{i,j}$ and the system becomes ordinary differential equations for the evolution of this cell ($\mathsf{D}_{i,j}$) average:

$$\frac{\partial \mathsf{W}_{i,j}}{\partial t} + \frac{1}{|\mathsf{D}|}\oint_{\partial \mathsf{D}} \big[(\mathsf{F} - \mathsf{R})dy + (\mathsf{G} - \mathsf{S})dx\big] = 0 \tag{5.4}$$

5.3 Artificial compressibility method

To compute incompressible, steady flow, it is necessary to solve the problem with absence of pressure in vector of unknowns $P\mathsf{W}$, if you like in continuity equation. Artificial compressibility method[3] is elegant method of solution of this problem. We can add time derivative of pressure to the continuity equation (2.15), which became zero, when the method converges to the steady solution:

$$\frac{1}{\beta^2}\frac{\partial p}{\partial \tau} + \frac{\partial u}{\partial x} + \frac{\partial v}{\partial y} = 0 \tag{5.5}$$

where β is artificial compressibility coefficient and represents local speed of sound of transformed system. The system (2.32) changes into:

$$\tilde{P}\mathsf{W}_t + \mathsf{F}_x + \mathsf{G}_y = \mathsf{R}_x + \mathsf{S}_y \tag{5.6}$$

where the only change is:

$$\tilde{P} = \begin{pmatrix} \frac{1}{\beta^2} & 0 & 0 \\ 0 & 1 & 0 \\ 0 & 0 & 1 \end{pmatrix}$$

We choose $\beta = 1$, then $\tilde{P} = I = diag(1, 1, 1)$ and our system of governing equations is independent on additional matrix $\tilde{P}$, so we will leave it out from our governing system for the rest of the work.

[3] e.g. Bodnár [2]

Chapter 6

Numerical method

Contents

6.1 Lax-Wendroff scheme

6.1.1 Derivation of Lax-Wendroff scheme

L-W scheme is based on the idea of Taylor expansions of the "new value" in time and substituting time derivatives by space derivatives[1]. Consider scalar equation:

$$\mathsf{W}_t + A\mathsf{W}_x = \mathbf{0} \tag{6.1}$$

We are looking for solution of type W_i^{n+1}:

$$\mathsf{W}_i^{n+1} = \mathsf{W}(x_i, t_{n+1}) = \mathsf{W}(x_i, t_n + \Delta t) \tag{6.2}$$

$$\mathsf{W}_i^{n+1} = \mathsf{W}_i^n + \mathsf{W}_t \Delta t + \mathsf{W}_{tt} \Delta t^2 + \mathcal{O}(\Delta t^3) \tag{6.3}$$

now, we replace time derivatives:

$$\begin{aligned}
\mathsf{W}_t &= -A\mathsf{W}_x, && (6.4)\\
\mathsf{W}_{tt} &= -A\mathsf{W}_{xt}, && (6.5)\\
\mathsf{W}_{tx} &= -A\mathsf{W}_{xx}, && (6.6)\\
\mathsf{W}_{tx} &= \mathsf{W}_{xt}, && (6.7)\\
\mathsf{W}_{tt} &= A^2\mathsf{W}_{xx} && (6.8)
\end{aligned}$$

[1] e.g. LeVeque [5]

then:

$$\mathsf{W}_i^{n+1} = \mathsf{W}_i^n - A\mathsf{W}_x\Delta t + A\mathsf{W}_{xx}\Delta t^2 \tag{6.9}$$

now, we discretize derivatives:

$$\mathsf{W}_i^{n+1} = \mathsf{W}_i^n - \frac{A\Delta t}{2\Delta x}(\mathsf{W}_{i+1} - \mathsf{W}_{i-1}) + \frac{A^2\Delta t^2}{2\Delta x^2}(\mathsf{W}_{i+1} - 2\mathsf{W}_i + \mathsf{W}_{i-1}) \tag{6.10}$$

Lax-Wendroff scheme is second order accurate:

$$\frac{T}{\Delta t}\mathcal{O}(\Delta t^3) \approx \mathcal{O}(\Delta t^2) \tag{6.11}$$

6.1.2 Modified equation for Lax-Wendroff scheme

All the second-order, three-point central schemes of the Lax-Wendroff family generate oscillations around sharp discontinuities[2]. Let us take a closer look at this problem. We start with constructing *modified equation* for Lax-Wendroff scheme. It can be find by substituting terms of Lax-Wendroff scheme (6.10) by its' Taylor expansions at point $\mathsf{W}(x_i, t_n)$.

The third-order Taylor expansions of individual terms of Lax-Wendroff scheme (6.10) are:

$$\mathsf{W}_i^{n+1} = \mathsf{W}(x_i, t_{n+1}) = \mathsf{W}(x_i, t_n) + \Delta t\mathsf{W}_t(x_i, t_n) + \frac{\Delta t^2}{2}\mathsf{W}_{tt}(x_i, t_n) + \frac{\Delta t^3}{6}\mathsf{W}_{ttt}(x_i, t_n) + \mathcal{O}(\Delta t^4) \tag{6.12}$$

$$\mathsf{W}_{i+1}^{n} = \mathsf{W}(x_{i+1}, t_n) = \mathsf{W}(x_i, t_n) + \Delta x\mathsf{W}_x(x_i, t_n) + \frac{\Delta x^2}{2}\mathsf{W}_{xx}(x_i, t_n) + \frac{\Delta x^3}{6}\mathsf{W}_{xxx}(x_i, t_n) + \mathcal{O}(\Delta x^4) \tag{6.13}$$

$$\mathsf{W}_{i-1}^{n} = \mathsf{W}(x_{i-1}, t_n) = \mathsf{W}(x_i, t_n) - \Delta x\mathsf{W}_x(x_i, t_n) + \frac{\Delta x^2}{2}\mathsf{W}_{xx}(x_i, t_n) - \frac{\Delta x^3}{6}\mathsf{W}_{xxx}(x_i, t_n) + \mathcal{O}(\Delta x^4) \tag{6.14}$$

. . . . . .

Now, we substitute these relations in Lax-Wendroff scheme (6.10):

$$\begin{aligned}\mathsf{W}(x_i, t_n) + \Delta t\mathsf{W}_t(x_i, t_n) + \frac{\Delta t^2}{2}\mathsf{W}_{tt}(x_i, t_n) + \frac{\Delta t^3}{6}\mathsf{W}_{ttt}(x_i, t_n) = \\ \mathsf{W}(x_i, t_n) - \frac{A\Delta t}{2\Delta x}\Big(2\Delta x\mathsf{W}_x(x_i, t_n) + \frac{\Delta x^3}{3}\mathsf{W}_{xxx}(x_i, t_n)\Big) \\ + \frac{A^2\Delta t^2}{2\Delta x^2}\Big(\Delta x^2\mathsf{W}_{xx}(x_i, t_n)\Big) + \mathcal{O}(\Delta t^4, \Delta x^4)\end{aligned} \tag{6.15}$$

that simplifies in:

$$\begin{aligned}\mathsf{W}_t(x_i, t_n) + A\mathsf{W}_x(x_i, t_n) = \\ -\frac{\Delta t}{2}\mathsf{W}_{tt}(x_i, t_n) - \frac{\Delta t^2}{6}\mathsf{W}_{ttt}(x_i, t_n) - \frac{A\Delta x^2}{6}\mathsf{W}_{xxx}(x_i, t_n) \\ + \frac{A^2\Delta t}{2}\mathsf{W}_{xx}(x_i, t_n) + \mathcal{O}(\Delta t^3, \Delta x^3)\end{aligned} \tag{6.16}$$

Using the same ideas as in section (6.1) we can continue:

$$\begin{aligned}\mathsf{W}_t(x_i, t_n) + A\mathsf{W}_x(x_i, t_n) = \\ -\frac{\Delta t^2}{6}\mathsf{W}_{ttt}(x_i, t_n) - \frac{A\Delta x^2}{6}\mathsf{W}_{xxx}(x_i, t_n) + \mathcal{O}(\Delta t^3, \Delta x^3) = \\ \frac{A^3\Delta t^2}{6}\mathsf{W}_{xxx}(x_i, t_n) - \frac{A\Delta x^2}{6}\mathsf{W}_{xxx}(x_i, t_n) + \mathcal{O}(\Delta x^3) = \\ -\frac{\Delta x^2}{6}\Big(A - \frac{\Delta t^2}{\Delta x^2}A^3\Big)\mathsf{W}_{xxx}(x_i, t_n) + \mathcal{O}(\Delta x^3)\end{aligned} \tag{6.17}$$

[2] Hirsh [7]

modified equation for Lax-Wendroff scheme:

$$\mathsf{W}_t + A\mathsf{W}_x = -\frac{\Delta x^2}{6}\Big(A - \frac{\Delta t^2}{\Delta x^2}A^3\Big)\mathsf{W}_{xxx} \tag{6.18}$$

One can see that modified equation of Lax-Wendroff scheme does not contain artificial viscosity of the second order. The term on the right hand side has dispersive character[3]. Hence, it is necessary to intensify the influence of artificial viscosity, to damp non-physical oscillations. One method to do that is using *additional artificial viscosity* ($D\mathsf{W}$). The additional artificial viscosity can be constructed by following way (Lax-Wendroff scheme):

$$\mathsf{W}_i^{n+1} = \mathsf{W}_i^n - \frac{A\Delta t}{2\Delta x}(\mathsf{W}_{i+1} - \mathsf{W}_{i-1}) + \frac{A^2\Delta t^2}{2\Delta x^2}(\mathsf{W}_{i+1} - 2\mathsf{W}_i + \mathsf{W}_{i-1}) + \underbrace{\Delta x^2\epsilon(\Delta x^a)(\mathsf{W}_{i+1} - 2\mathsf{W}_i + \mathsf{W}_{i-1})}_{D\mathsf{W} = \text{additional artificial viscosity term}} \tag{6.19}$$

where $\epsilon > 0$ is coefficient of additional artificial viscosity.

Modified equation is then:

$$\mathsf{W}_t + A\mathsf{W}_x = \Delta x^2\epsilon(\Delta x^a)\mathsf{W}_{xx} - \frac{\Delta x^2}{6}\Big(A - \frac{\Delta t^2}{\Delta x^2}A^3\Big)\mathsf{W}_{xxx} \tag{6.20}$$

Now, the modified equation contains the member with second derivative, that damps oscillations and helps to keep stability of method.

6.2 MacCormack scheme

MacCormack scheme is a two-step scheme. This is a formulation of Lax-Wendroff scheme in the form *predictor-corrector*. Both schemes became identic in case of linear problem solution. It is an iteration method, that works in three steps. At first, the predictor step (6.21) is computed, and from "new values" is then the second, corrector step (6.22), computed. In the third step additional artificial viscosity (artificial dissipation) is added. Then the next iteration follows, until the solution is converged. Inviscid and viscous fluxes are evaluated[4] different way, according to Sections 6.2.1 and 6.2.2 and figures 6.2 and 6.3.

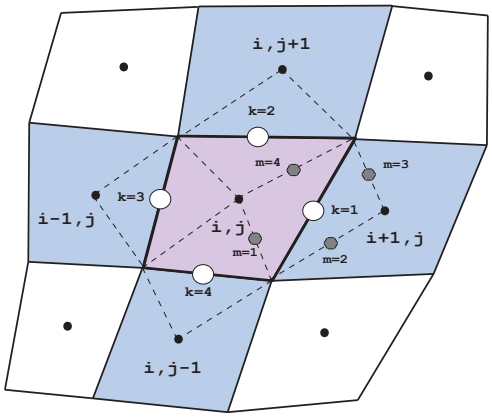

Figure 6.1: Computational stencil for Finite volume method

[3] [8]
[4] Following Bodnár [2]

Predictor

$$\mathsf{W}_{i,j}^{n+\frac{1}{2}} = \mathsf{W}_{i,j}^{n} - \frac{\Delta t}{|\mathsf{D}_{i,j}|}\sum_{k=1}^{4}\{(\mathsf{F}_k^n - \mathsf{R}_k^n)\Delta y_k - (\mathsf{G}_k^n - \mathsf{S}_k^n)\Delta x_k\} \tag{6.21}$$

Corrector (+ Predictor)

$$\left(\mathsf{W}_{i,j}^{n+1}\right) = \frac{1}{2}\left(\mathsf{W}_{i,j}^{n} + \mathsf{W}_{i,j}^{n+\frac{1}{2}} - \frac{\Delta t}{|\mathsf{D}_{i,j}|}\sum_{k=1}^{4}\{(\mathsf{F}_k^{n+\frac{1}{2}} - \mathsf{R}_k^{n+\frac{1}{2}})\Delta y_k - (\mathsf{G}_k^{n+\frac{1}{2}} - \mathsf{S}_k^{n+\frac{1}{2}})\Delta x_k\}\right) \tag{6.22}$$

Corrector (+ Predictor) + Artificial viscosity

$$\mathsf{W}_{i,j}^{n+1} = \left(\mathsf{W}_{i,j}^{n+1}\right) + \mathsf{DW}_{i,j}^{n} \tag{6.23}$$

6.2.1 Discretization of inviscid fluxes

Predictor $\mathsf{F}_1 = \mathsf{F}_2 = \mathsf{F}_{i,j}, \mathsf{F}_3 = \mathsf{F}_{i-1,j}, \mathsf{F}_4 = \mathsf{F}_{i,j-1}$

- also applies to G.

Corrector $\mathsf{F}_1 = \mathsf{F}_{i+1,j}, \mathsf{F}_2 = \mathsf{F}_{i,j+1}, \mathsf{F}_3 = \mathsf{F}_4 = \mathsf{F}_{i,j}$

-also applies to G.

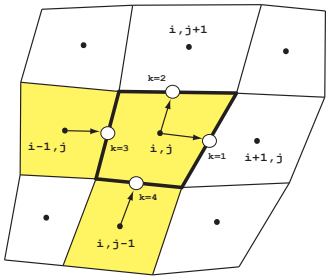

(a) Predictor - backward step

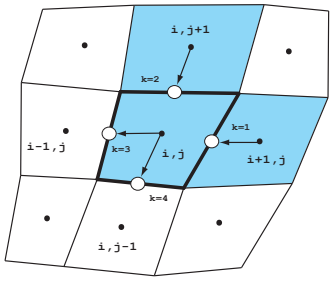

(b) Corrector - forward step

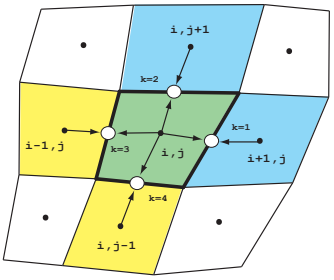

(c) Predictor + Corrector

Figure 6.2: Stencil for inviscid fluxes computation

6.2.2 Discretization of viscous fluxes

Derivatives of velocity for viscous fluxes we can get from integration over dual cell boundary (6.24) figure 6.3. Integral is replaced by discrete sum over dual cell faces:

$$u_x \approx \frac{1}{\mathsf{D}_m} \oint_{\partial D} u\nu^x dxdy \approx \frac{1}{\mathsf{D}_m} \sum_{m=1}^{4} u_m \nu_m^x l_m \tag{6.24}$$

where: u_m is velocity in the center of the m-th face, ν_m^x is outer normal of the face, l_m is length of the face, D_m is area of a dual cell. Values of variables in the middle of dual faces are computed as an average of values of its neighbor values. The member $\mathsf{DW}_{i,j}^n$ is artificial viscosity and is added to corrector to damp oscillations. We will discuss details in Section (6.3).

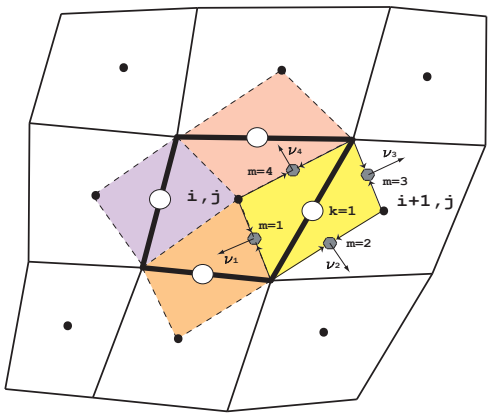

Figure 6.3: Stencil for viscous fluxes computation (dual cells)

6.3 Artificial viscosity

We have used two different types of artificial viscosity. The first one is Von Neumann - Richtmayer (Von Neumann & Richtmayer, 1950) artificial viscosity, that is traditional and proven artificial viscosity. The second one is artificial viscosity with TVD abitlity[5]. The whole scheme is then called TVD MacCormack scheme.

6.3.1 Von Neumann - Richtmayer artificial viscosity

It was used in form[6] (1D case for simplicity):

$$\mathsf{DW}_i^n = \epsilon_2 \Delta x^3 \frac{d}{dx} |\mathsf{W}_x| \mathsf{W}_x \Big|_i^n + \epsilon_4 \Delta x^4 \mathsf{W}_{xxxx} \Big|_i^n \tag{6.25}$$

After replacing derivations we obtain:

$$\mathsf{DW}_i^n = \epsilon_2 \left[|\mathsf{W}_{i+1}^n - \mathsf{W}_i^n| (\mathsf{W}_{i+1}^n - \mathsf{W}_i^n) - |\mathsf{W}_i^n - \mathsf{W}_{i-1}^n| (\mathsf{W}_i^n - \mathsf{W}_{i-1}^n) \right] + \epsilon_4 (\mathsf{W}_{i-2}^n - 4\mathsf{W}_{i-1}^n + 6\mathsf{W}_i^n - 4\mathsf{W}_{i+1}^n + \mathsf{W}_{i+2}^n) \tag{6.26}$$

where $\epsilon_2, \epsilon_4 \in \mathbb{R}$ are constants, that have to be carefully chosen.

[5] e.g. Fürst [4]
[6] Hirsh [7]

6.3.2 Modified Causon's TVD MacCormack scheme

We mention 1D case[7] again, for simplicity, two dimensional artificial viscosity is analogical and the second direction varies in indices only:

$$\mathsf{DW}_i^n = \left[\bar{G}^+(\bar{r}_i^+) + \bar{G}^-(\bar{r}_{i+1}^-)\right]\left(\mathsf{W}_{i+1}^n - \mathsf{W}_i^n\right) - \left[\bar{G}^+(\bar{r}_{i-1}^+) + \bar{G}^-(\bar{r}_i^-)\right]\left(\mathsf{W}_i^n - \mathsf{W}_{i-1}^n\right) \tag{6.27}$$

where:

$$\bar{r}_i^+ = \frac{< \mathsf{W}_i^n - \mathsf{W}_{i-1}^n, \mathsf{W}_{i+1}^n - \mathsf{W}_i^n >}{< \mathsf{W}_{i+1}^n - \mathsf{W}_i^n, \mathsf{W}_{i+1}^n - \mathsf{W}_i^n >} \tag{6.28}$$

$$\bar{r}_i^- = \frac{< \mathsf{W}_i^n - \mathsf{W}_{i-1}^n, \mathsf{W}_{i+1}^n - \mathsf{W}_i^n >}{< \mathsf{W}_i^n - \mathsf{W}_{i-1}^n, \mathsf{W}_i^n - \mathsf{W}_{i-1}^n >} \tag{6.29}$$

Here $< \cdot, \cdot >$ denotes the standard inner scalar product.

$$\bar{G}^+(\bar{r}_i^+) = \frac{1}{2}C(\bar{\nu}_i)[1 - \Phi(\bar{r}^+)] \tag{6.30}$$

$$\bar{G}^+(\bar{r}_i^-) = \frac{1}{2}C(\bar{\nu}_i)[1 - \Phi(\bar{r}^-)] \tag{6.31}$$

$$\Phi(\bar{r}^\pm) = \max(0, \min(2\bar{r}^\pm, 1)) \tag{6.32}$$

$$C(\bar{\nu}_i) = \begin{cases} \bar{\nu}_i(1 - \bar{\nu}_i) & \text{for } \bar{\nu}_i \leq 0.5 \\ 0.25 & \text{for } \bar{\nu}_i > 0.5 \end{cases} \tag{6.33}$$

$$\bar{\nu}_i = \Psi(a_i)\frac{\Delta t}{\Delta x} \tag{6.34}$$

$$a_i = \min \begin{cases} \dfrac{un_x + vn_y}{} \\ un_x + vn_y + \sqrt{u^2n_x^2 + 2un_xvn_y + v^2n_y^2 + n_x^2 + n_y^2} \\ un_x + vn_y - \sqrt{u^2n_x^2 + 2un_xvn_y + v^2n_y^2 + n_x^2 + n_y^2} \end{cases} \tag{6.35}$$

$$\Psi(a_i) = \begin{cases} |a_i| & \text{for } |a_i| > \epsilon_e \\ \frac{a_i^2 + \epsilon_e^2}{2\epsilon_e} & \text{for } |a_i| \leq \epsilon_e \end{cases} \tag{6.36}$$

where a_i is minimal absolute value of eigenvalues of the Jacobi matrix A_i at the point W_i. $\Psi(a_i)$ is called entropy correction with $\epsilon_e = 10^{-3}$

6.4 Time step restrictions

To keep stability of the method, it is important to find correct time step of the method. Time step is computed always for each iteration. For cartesian mesh time step can be computed from the following relation:

$$\Delta t = min\frac{CFL}{\frac{\rho_a}{\Delta x} + \frac{\rho_b}{\Delta y} + \left(\frac{1}{Re} + \frac{1}{Re_T}\right)\left(\frac{1}{\Delta x^2} + \frac{1}{\Delta y^2}\right)} \tag{6.37}$$

where Re is Reynolds number, $Re_T = \frac{\nu}{\nu_T}$ is Turbulent Reynolds number, $CFL \leq 1$ is called *Courant* number, ρ_a and ρ_b are spectral radii of jacobian of inviscid fluxes F and G:

$$\rho_a = |u| + \sqrt{u^2 + \beta^2}, \quad \rho_b = |v| + \sqrt{v^2 + \beta^2} \tag{6.38}$$

[7] e.g. Fürst [4]

In most cases it is useful to use *Local Time Stepping* method. It is acceleration method, based on the idea that time step is used for each cell separately ($\Delta t \rightarrow \Delta t_{i,j}$). As a result, each cell has its own iteration time, but it does not harm the final solution, because of its steady character. This technique can shorten iteration time even to one half. But one should keep on mind taking risk of some possibility of lost of consistency leading to breaking up stability.

6.5 Monitoring of convergency

For monitoring of convergency of conservative components we have used[8] global $L_2 - norm$. Consider $Rez \sim \|Rez(W)\|_{L_2}$ which in ideal case should come close to zero.

$$Rez = \sqrt{\sum_{i,j} \frac{1}{M \cdot N} \Big(\frac{\mathsf{W}_{i,j}^{n+1} - \mathsf{W}_{i,j}^{n}}{\Delta t} \Big)^2} \tag{6.39}$$

For example figure 7.12 shows residual history of iteration process from the test case C_1.

[8] e.g. Kozel & Dvořák [1]

Chapter 7

Application

Contents

7.1 Realization of problem solution

7.1.1 Data organization

In all solved test cases, we have used structured mesh and sorting data of type $cell - centered$ (the values are kept in the center of the cell). Variables are set in two dimensional fields as shows figure 7.1. Colored fields indicate some possible ways of variable organization at the boundary of computational domain. The way of variable organization depends on the appropriate boundary condition.

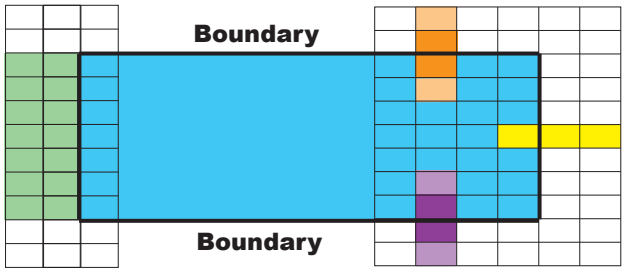

Figure 7.1: Data organization

7.1.2 General test case set

Figure 7.2 shows general computational domain. Each domain usually consists of:

- **Inlet:** In the most common variant, at the inlet, the velocity (either constant, or parabolic profile) is kept constant the pressure is extrapolated from the inside of computational domain. In general the number of extrapolated variables depends on the normal velocity component compared with the local speed of sound. If the normal inlet velocity component is greater than the local speed of sound, all the variables are kept and none is extrapolated from the inside.
- **Outlet:** The pressure is kept constant and the rest of variables are extrapolated from the inside of computational domain. If the normal inlet velocity component is greater than the local speed of sound, none variable is kept constant and all the variables are extrapolated from the inside.
- **Wall:** Here the boundary condition depends on the type of boundary. The most common type of boundary is either *viscous wall* (no-slip condition, velocity equals zero, $\boldsymbol{v} = 0$), or *symmetry* (free-slip condition, normal component of velocity equals to zero, $\boldsymbol{v} \cdot \vec{n} = 0$) or the combination of them.

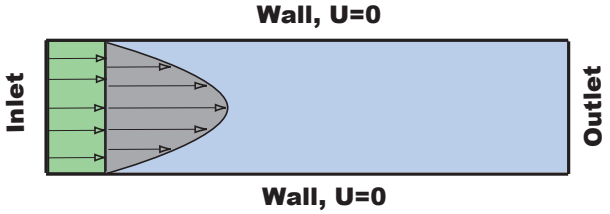

Figure 7.2: General test case set-up

7.2 Computational domains for non-Newtonian test cases

7.2.1 Gap between two flat plates

The simplest geometry, we have used, is the gap between two flat plates and we will call it straight channel. The diameter of the straight channel is $D = 10.0\ mm$ and $L = 10D$.

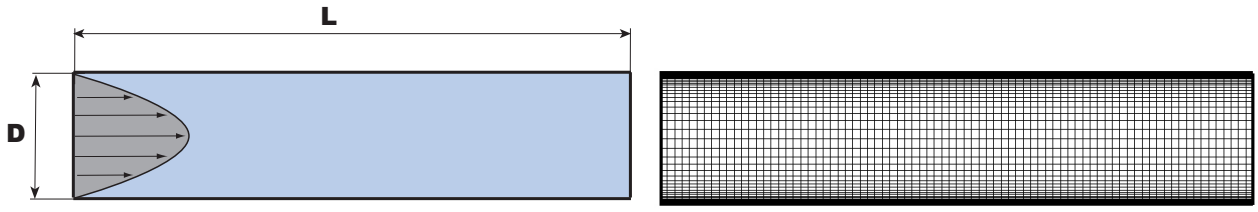

(a) The geometry of the gap between two flat plates (b) Mesh: 80x50 cells

Figure 7.3: Gap between two flat plates

7.2.2 Narrowed channel

Another computational domain is a narrowed channel, simulating blood vessel stenosis :

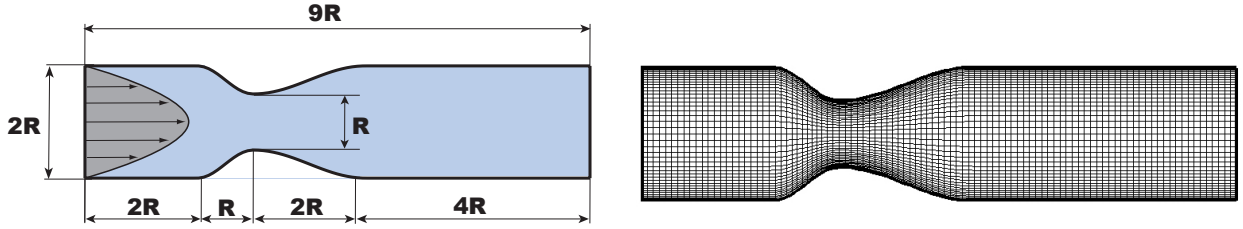

(a) Narrowed channel geometry (b) Narrowed channel mesh: 100x40 cells

Figure 7.4: Narrowed channel

The channel is axisymmetric and the narrowed part is of cosine shape. The diameter is $D = 2R = 10.0\ mm$. In the narrowed part the velocity increases and stream accelerates.

7.2.3 Widened channel

Another computational domain is a widened channel, simulating blood vessel aneurism :

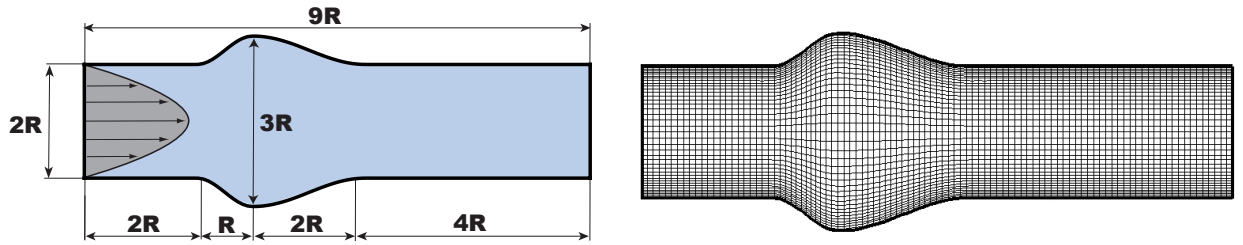

(a) Widened channel geometry (b) Widened channel mesh: 100x40 cells

Figure 7.5: Widened channel

The channel is as well axisymmetric and the widened part is of cosine shape. The diameter is $D = 2R = 10.0\ mm$. In the widened part the velocity decreases and stream decelerate.

7.2.4 Curved channel

Another computational domain is a curved channel with constant curvature. The diameter is $D = 10.0\ mm$, $R = 30\ mm$, $L_1 = L_2 = 20\ mm$.

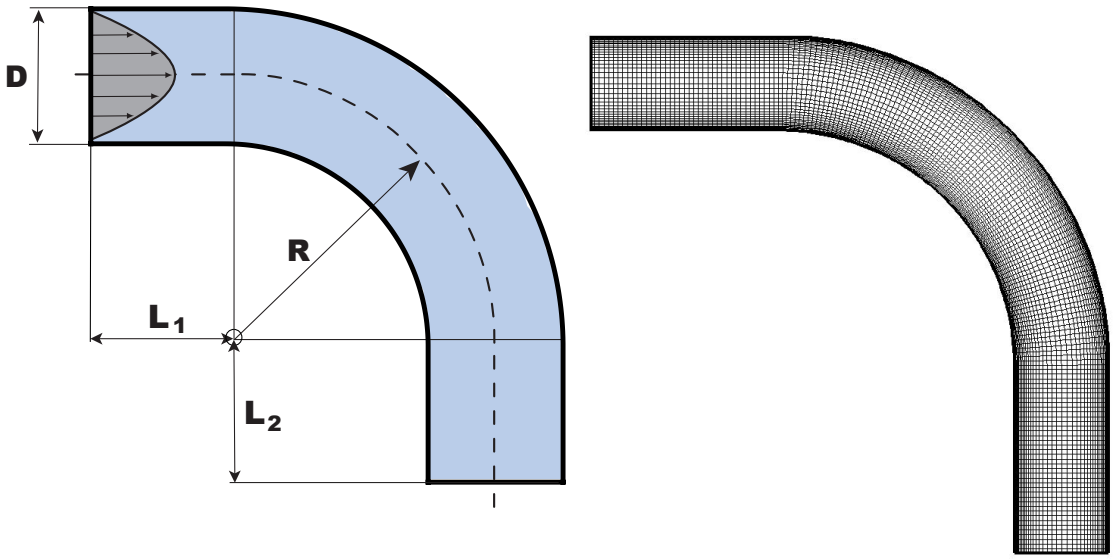

(a) Curved channel geometry (b) Curved channel mesh: 170x40

Figure 7.6: Curved channel

7.2.5 Meshes for test cases

All the meshes used in this work, except the two flat plate meshes, were generated by author partly in *C++*, partly in *Tecplot 10.0*. The theory of mesh generating is very extensive and is beyond the objective of this work. Here, we put up with general rules for mesh generating. All the meshes were generated to be *smooth*[1] enough and *wall fitted*[2] with afford to place more cells in the boundary layer.

[1] the difference of the cells' lengths between two following cells is $\leq 20\%$ in each direction
[2] to catch large velocity gradients

7.3 Validation of method

Validation of the method is very important and gives us an idea of method accuracy and application possibilities. The first two test cases in this work are aimed on validation of the method. In the test cases C_1 and C_2 the comparison of our method solution with analytical solution was made. In the test cases $\mathsf{C}_7, \mathsf{C}_8$ and C_9 the comparison of our method solution with renowned measurements was made.

7.3.1 C_1 : Velocity profile in the gap between two plates

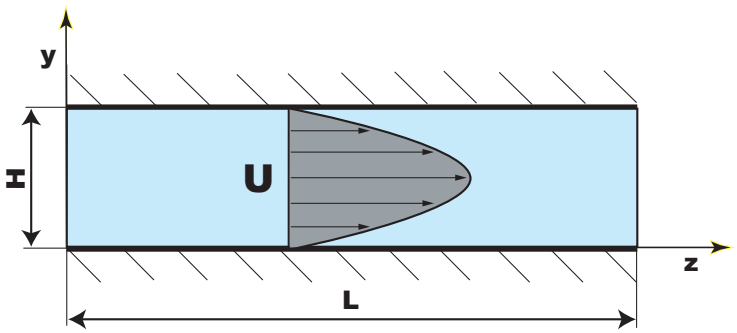

Figure 7.7: Gap between two plates

Let us try to find exact solution of velocity distribution in the gap between two endless plates (straight channel, figure 7.7). Let us consider Navier-Stokes equations for incompressible, viscous, newtonian fluid:

$$\frac{\partial u}{\partial x} + \frac{\partial v}{\partial y} + \frac{\partial w}{\partial z} = 0 \tag{7.1}$$

$$\rho\Big(\frac{\partial u}{\partial t} + u\frac{\partial u}{\partial x} + v\frac{\partial u}{\partial y} + w\frac{\partial u}{\partial z}\Big) = -\frac{\partial p}{\partial x} + \mu\Big(\frac{\partial^2 u}{\partial x^2} + \frac{\partial^2 u}{\partial y^2} + \frac{\partial^2 u}{\partial z^2}\Big) \tag{7.2}$$

$$\rho\Big(\frac{\partial v}{\partial t} + u\frac{\partial v}{\partial x} + v\frac{\partial v}{\partial y} + w\frac{\partial v}{\partial z}\Big) = -\frac{\partial p}{\partial y} + \mu\Big(\frac{\partial^2 v}{\partial x^2} + \frac{\partial^2 v}{\partial y^2} + \frac{\partial^2 v}{\partial z^2}\Big) \tag{7.3}$$

$$\rho\Big(\frac{\partial w}{\partial t} + u\frac{\partial w}{\partial x} + v\frac{\partial w}{\partial y} + w\frac{\partial w}{\partial z}\Big) = -\frac{\partial p}{\partial z} + \mu\Big(\frac{\partial^2 w}{\partial x^2} + \frac{\partial^2 w}{\partial y^2} + \frac{\partial^2 w}{\partial z^2}\Big) \tag{7.4}$$

We will consider the flow in direction z , $(u = v = 0)$. Continuity equation (7.1) is then:

$$\frac{\partial w}{\partial z} = 0 \tag{7.5}$$

Momentum equations(7.2),(7.3) and (7.4) become:

$$\rho w\frac{\partial w}{\partial z} = -\frac{\partial p}{\partial z} + \mu\Big(\frac{\partial^2 w}{\partial x^2} + \frac{\partial^2 w}{\partial y^2} + \frac{\partial^2 w}{\partial z^2}\Big) \tag{7.6}$$

We know, that $\partial w/\partial x$ is 0 for this case of endless desks. Using equation (7.5), the equation (7.6) can be simplified:

$$\mu\frac{\partial^2 w}{\partial y^2} = \frac{\partial p}{\partial z} \tag{7.7}$$

where pressure gradient can be substituted by ratio of pressure difference Δp and distance L:

$$\frac{\partial^2 w}{\partial y^2} = \frac{1}{\mu}\frac{\Delta p}{L} \tag{7.8}$$

To get velocity profile w, we can integrate:

$$w = \frac{1}{\mu}\frac{\Delta p}{L}\frac{y^2}{2} + C_1 y + C_2 \tag{7.9}$$

Now, we can add boundary conditions, to get integration constants:

$$w = 0, \quad for \quad y = 0 \tag{7.10}$$

$$w = 0, \quad for \quad y = H \tag{7.11}$$

then:

$$C_1 = 0, \quad C_2 = -\frac{1}{\mu}\frac{\Delta p}{L}\frac{H}{2} \tag{7.12}$$

Now, we have the exact equation for velocity profile in the gap between two plates:

$$w = \frac{1}{2\mu}\frac{\Delta p}{L}(y^2 - Hy) \tag{7.13}$$

Test case: Our numerical method was applied on the following test case. Used geometry is the straight channel introduced in figure 7.3. We want to compare numerical solution with exact solution given by equation (7.13). Used constants are: $L = 4.5$, $H = 1.0$, $\Delta p = 1.0$, $\mu = 0.01$, $\rho = 1$. At the inlet was kept constant pressure ($p = 1.0$) and velocity components were extrapolated. At the outlet was kept constant pressure ($p = 0.0$) and velocity components were extrapolated.

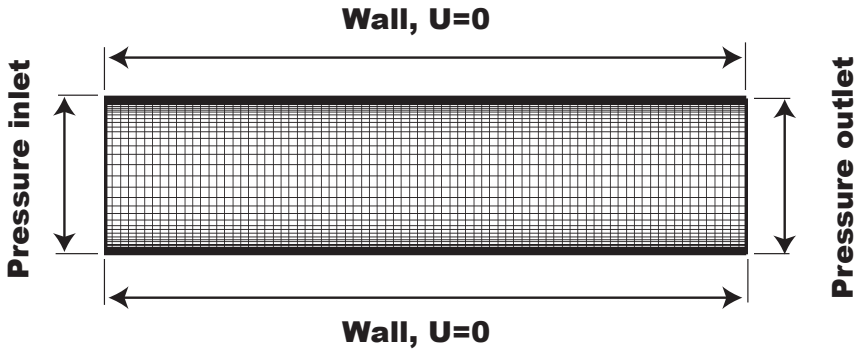

Figure 7.8: Computational domain

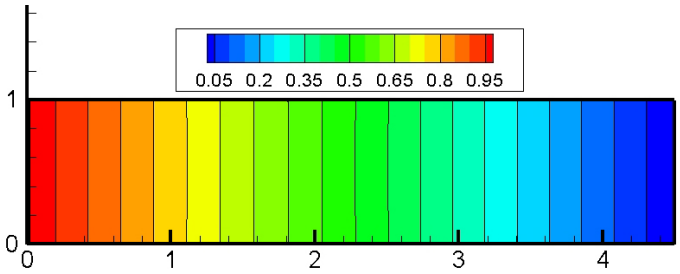

Figure 7.9: Pressure magnitude

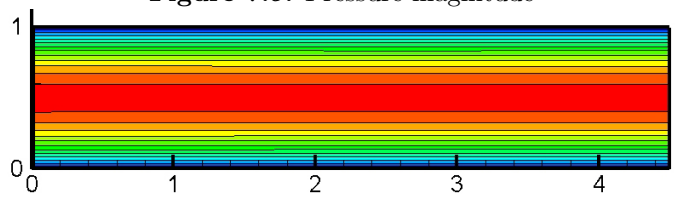

Figure 7.10: Absolute velocity magnitude

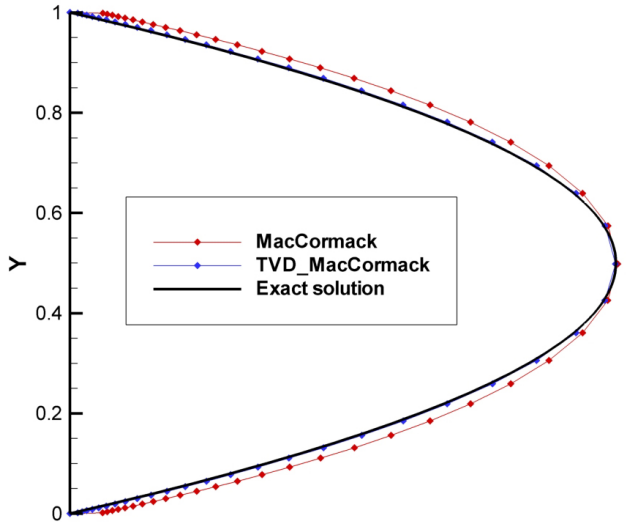

Figure 7.11: Comparison of velocity profiles

Results: Pressure magnitude (figure 7.9) is, as expected, linearly spread from inlet to outlet. Velocity magnitude (figure 7.10) is , as expected, of the same parabolic profile in all the computational domain. Figure 7.11 shows final comparison of exact solution and two computed schemes, the first one is MacCormack scheme with "ordinary" artificial viscosity introduced in Section 6.3.1 and the second one is TVD MacCormack scheme introduced in Section 6.3.2.

Solution showed that the first method is very sensitive on choice of artificial viscosity coefficients. The second method is a little bit more time consuming, but closer to exact solution. Figure 7.12 shows residual history of iteration process for u-component of velocity. The blue color belongs to TVD MacCormack scheme and the red color belongs to the MacCormack scheme.

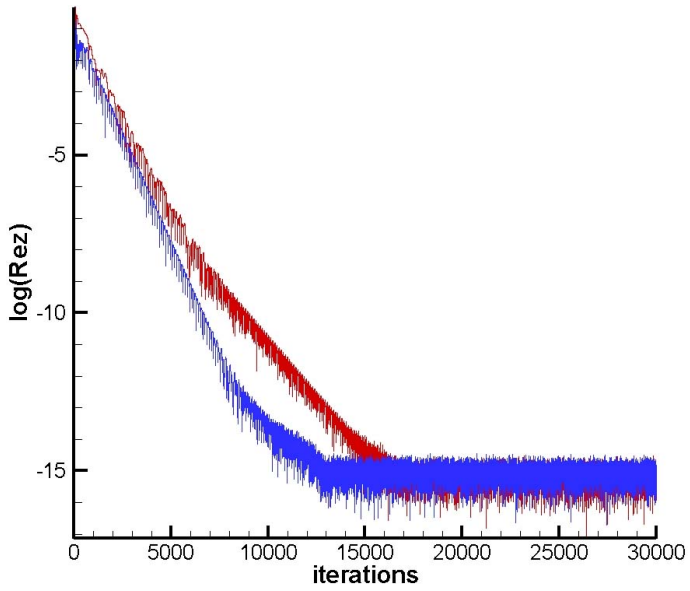

Figure 7.12: u-component residual history of iteration process

Figure 7.12 shows residual history of iteration process from the test case C_1. All the residual histories look similarly so we will not mention them anymore.

7.3.2 C_2 : Comparison of friction coefficient c_f

Another important validation of the method for viscous flow is comparison of friction coefficient c_f. It is in general the ratio of the weight of an object being moved along a surface and the force that maintains contact between the object and the surface. It can be expressed:

$$c_f = \frac{2\tau_w}{\rho_\infty v_\infty^2} \tag{7.14}$$

We have realized solution on the endless flat plate. Reynolds number of flow is $Re = 200000$. Figure 7.14 shows the computational domain of the tested case. The desk begins at the origin and ends at the point [1,0].

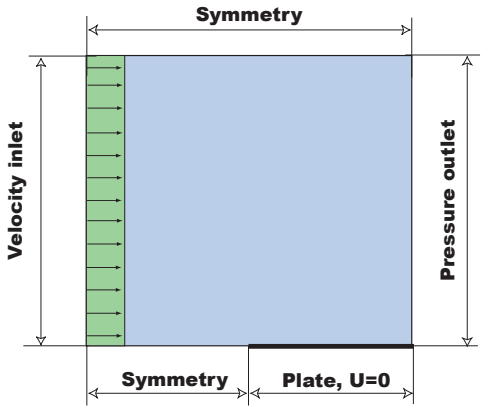

Figure 7.13: Flat plate computational domain

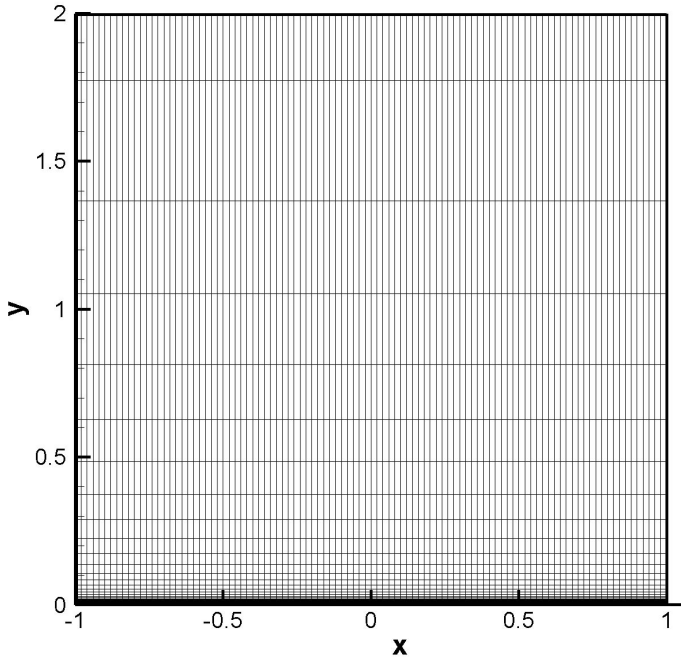

Figure 7.14: The flat plate mesh, 100x41 cells

Results: Figure 7.15 shows final comparison of exact solution and two computed schemes, the first one is MacCormack scheme with "ordinary" artificial viscosity (6.3.1) and the second one is TVD MacCormack scheme (6.3.2). Figure 7.15 (a) shows comparison of our c_f profiles with exact solution. Figure 7.15 (b) shows comparison of our velocity profile in the developed boundary layer ($x = 0.9$) with the exact solution.

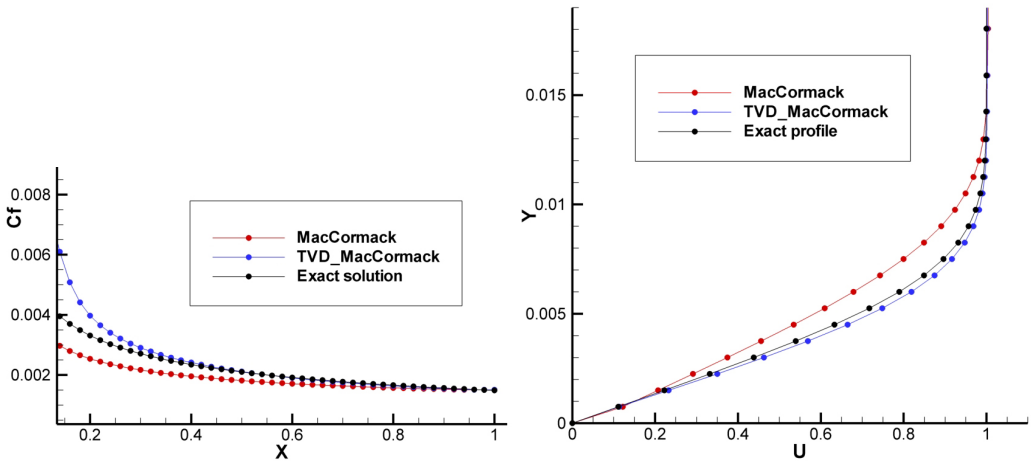

(a) Comparison of friction coefficientc_f (b) Comparison of velocity profiles

Figure 7.15: Laminar plate results

The both numerical methods we have introduced give similar results. The Causon's Modified TVD MacCormack scheme showed out a bit better results. Thus, for all the following test cases we will use this method only.

7.4 Non-Newtonian test cases

7.4.1 C_3 : Comparison of non-Newtonian viscosity models on narrowed channel

The non-Newtonian viscosity models we decided to compare on narrowed channel introduced in Section (7.2.2). Figure 7.16 shows comparison of non-Newtonian viscosity models from Section (3.2.2). The flow conditions of the test case are set to simulate the human blood behavior. For reference Newtonian case we have used infinity shear viscosity $\eta_\infty = 0.00345\ Pa.s$. The inlet velocity is $U = 6.15\ cm.s^{-1}$. The density is $\rho = 1050\ kg/m^3$. All models give similar results. For other following test cases of non-Newtonian flows we will use Modified Cross Model, if not mentioned details.

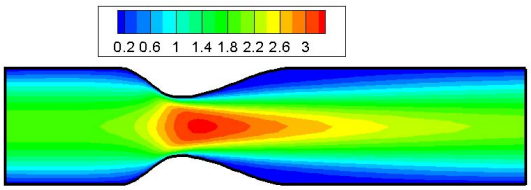

(a) Newtonian, velocity magnitude

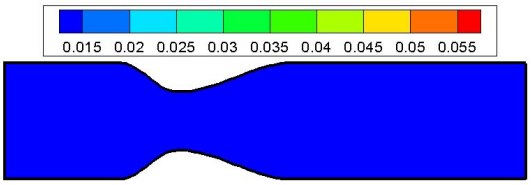

(b) Newtonian, viscosity magnitude

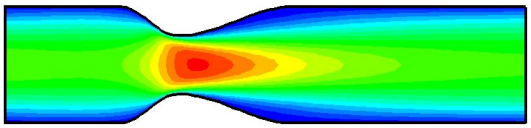

(c) Power Law Model, velocity magnitude

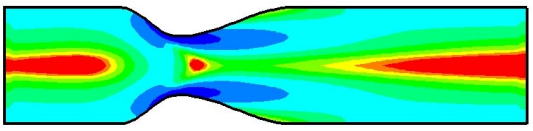

(d) Power Law Model, viscosity magnitude

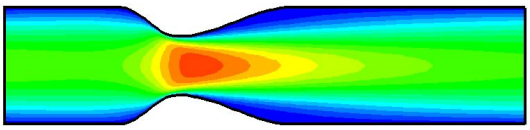

(e) Modified Cross Model, velocity magnitude

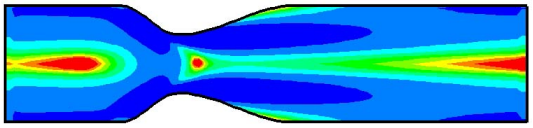

(f) Modified Cross Model, viscosity magnitude

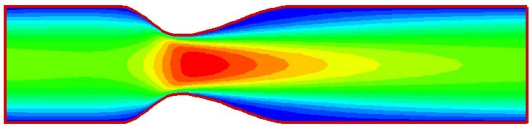

(g) Powel-Eyring model, velocity magnitude

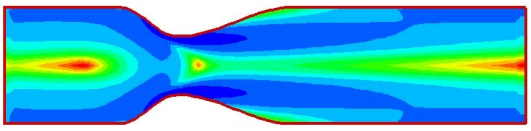

(h) Powel-Eyring model, viscosity magnitude

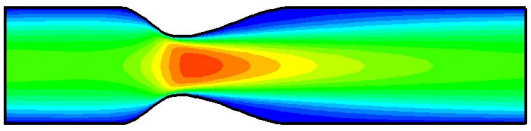

(i) Modified Powel-Eyring model, velocity magnitude

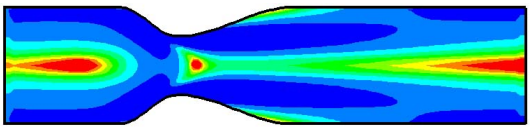

(j) Modified Powel-Eyring model, viscosity magnitude

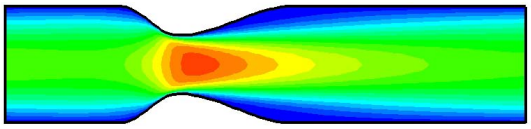

(k) Cross Model, velocity magnitude

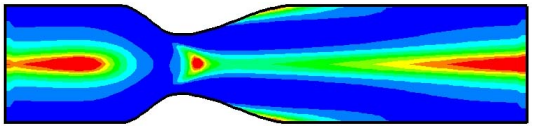

(l) Cross Model, viscosity magnitude

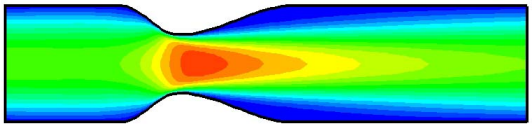

(m) Simplified Cross Model, velocity magnitude

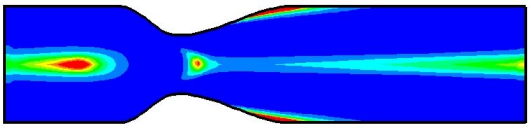

(n) Simplified Cross Model, viscosity magnitude

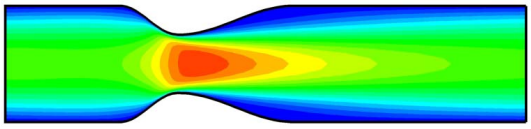

(o) Carreau Model, velocity magnitude

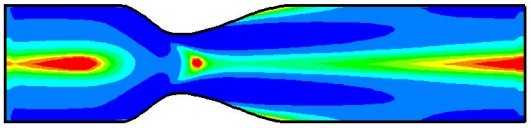

(p) Carreau Model, viscosity magnitude

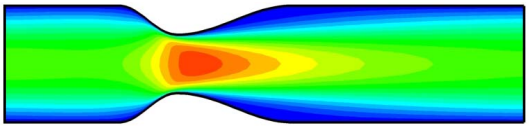

(q) Carreau-Yasuda Model, velocity magnitude

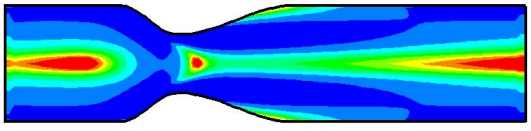

(r) Carreau-Yasuda Model, viscosity magnitude

Figure 7.16: Comparison of non-Newtonian viscosity models

7.5 Comparison of Newtonian and non-Newtonian flow

7.5.1 C_4 : Velocity magnitude difference

Let us take a look at the straight channel introduced in Figure 7.3. As was written, there are some differences between Newtonian and non-Newtonian flows. The first one is the difference in developed velocity profile. Figure 7.17 shows comparison of Newtonian and non-Newtonian flows. At the inlet is given velocity $U = 6.15\ cm.s^{-1}$ of Newtonian profile given by equation (7.13). The coefficients of non-Newtonian model[3] are set for human blood and reference viscosity for Newtonian flow is infinity shear viscosity ($\eta = \eta_\infty = 0.00345 Pa.s$). Figure 7.18 shows comparison of velocity at the end of the channel. One can see that non-Newtonian flow is slower in the middle of the channel because of the increase of viscosity in that place, but faster in places with greater gradients, where the particles could be interpreted to be cut by the flow.

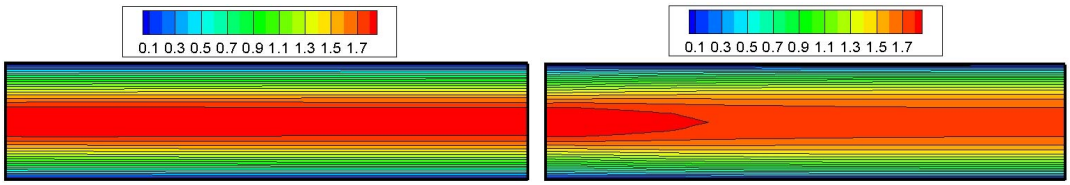

(a) Newtonian flow, velocity magnitude (b) non-Newtonian flow, velocity magnitude

Figure 7.17: Comparison of Newtonian and non-Newtonian velocity magnitude

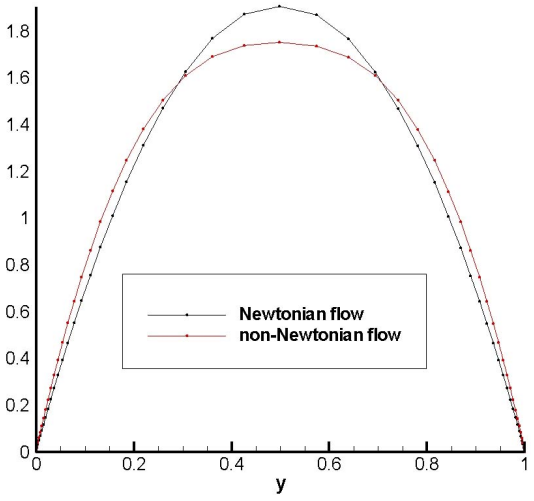

(a) Velocity profiles

Figure 7.18: Comparison of both velocity profiles at the end of the channel

[3] Modified Cross Model

7.5.2 C_5 : Pressure distribution difference

Now, let us make comparison of pressure distribution of Newtonian and non-Newtonian flows on the widened channel and on the curved channel.

At the inlet is given velocity $U = 6.15\ cm.s^{-1}$ of Newtonian flow profile given by equation (7.13). The coefficients of non-Newtonian model[4] are set for human blood and reference viscosity for Newtonian flow is infinity shear viscosity ($\eta = \eta_\infty = 0.00345\ Pa.s$). Figure 7.19 shows pressure comparison of Newtonian and non-Newtonian flows on the widened channel. The pressure generated at the inlet in the non-Newtonian case is greater, but its clear because the viscosity only increases against the Newtonian case.

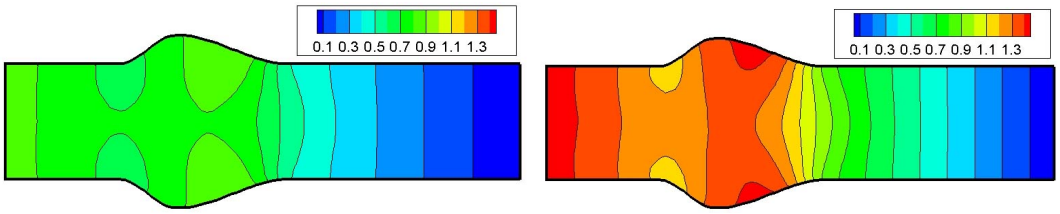

(a) Newtonian flow, pressure distribution (b) non-Newtonian flow, pressure distribution

Figure 7.19: Comparison of Newtonian and non-Newtonian pressure distribution

Following figures shows pressure magnitude comparison on the curved channel, but here the reference viscosity for Newtonian flow is ($\eta = 0.01\ Pa.s$) with afford to be close to blood behavior like in non-Newtonian case.

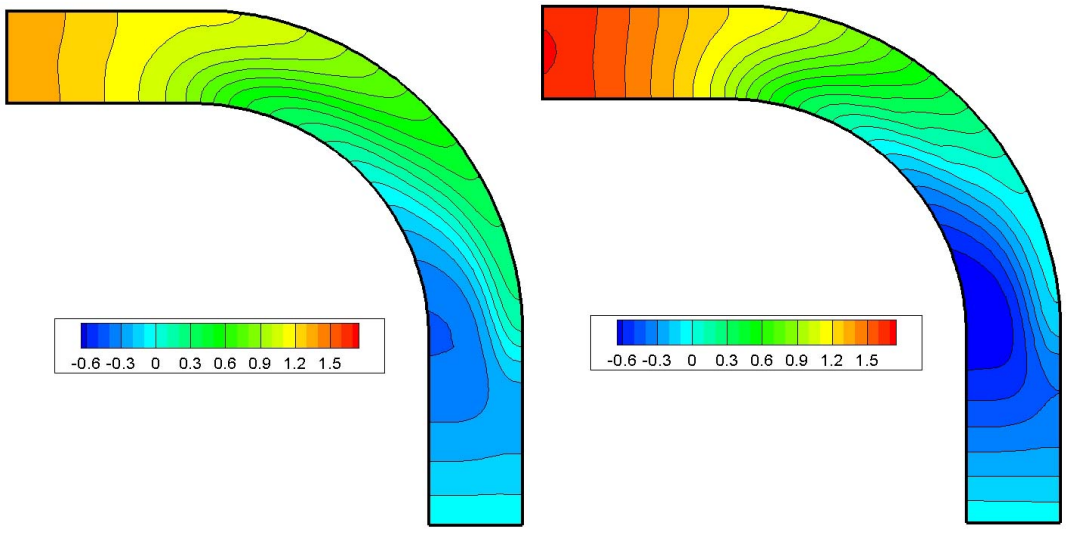

(a) Newtonian flow, pressure distribution (b) non-Newtonian flow, pressure distribution

Figure 7.20: Comparison of Newtonian and non-Newtonian pressure magnitude

[4]Modified Cross Model

7.5.3 C_6 : Comparison Newtonian and non-Newtonian flows on curved channel

Let us take a look at comparison of Newtonian and non-Newtonian[5] flow on the curved channel introduced in Section (7.2.4). The flow conditions are the same as in the previous cases, only the reference viscosity for Newtonian flow ($\eta_{ref} = 0.01\ Pa.s$) with afford to be close to blood behavior like in non-Newtonian case. This times we would like to show the comparison by special way. We made three dimensional model, where two space dimensions are completed by the third direction which is represented by variable we analyzing. Figure 7.21 shows velocity magnitude. The red colored profile denotes the non-Newtonian flow and the blue profile denotes the Newtonian flow. One can easily see in which regions each of the flows dominates. Figure 7.22 shows in which regions the non-Newtonian or Newtonian viscosity dominates. In the blue region the Newtonian viscosity dominates ($\eta_{ref} > \eta$), in the red region the non-Newtonian viscosity dominates ($\eta_{ref} \leq \eta$).

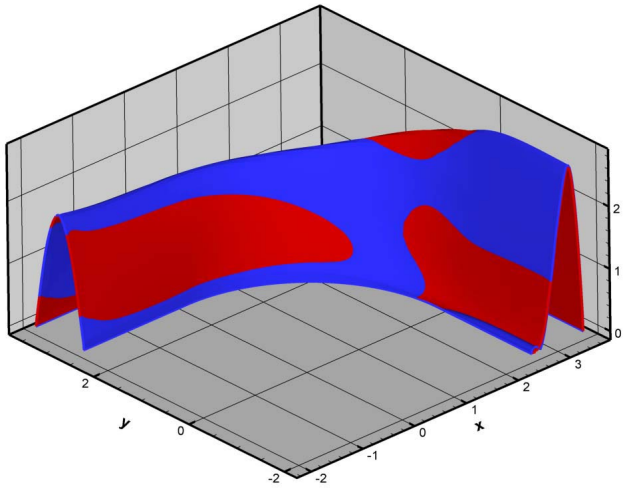

Figure 7.21: Comparison of velocity magnitude

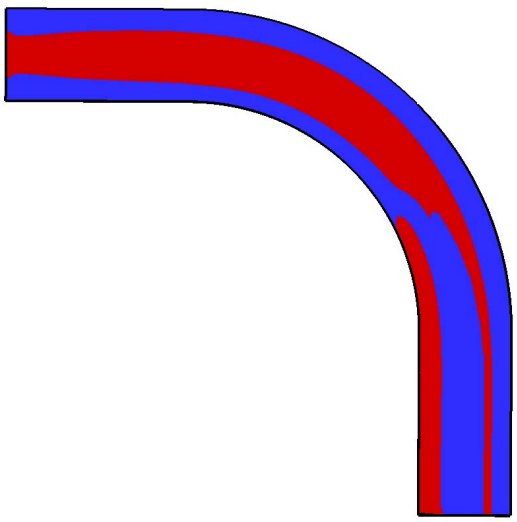

Figure 7.22: Dominate viscosity regions

[5]Modified Cross Model

7.6 Turbulent test cases

Turbulence modelling is complicated phenomenon. Requirements on the mesh quickly increase with Reynolds number. To catch turbulent boundary layer the mesh should have placed at least fifteen cells in range of δ at the wall. Thick mesh leads to great increase of requirements of computational time.

7.6.1 C_7 : Turbulent flow around the flat plate

The first test case is the flat plate. Boundary conditions are the same as in C_2. $Re = 500000$. Computational domain shows the following figure:

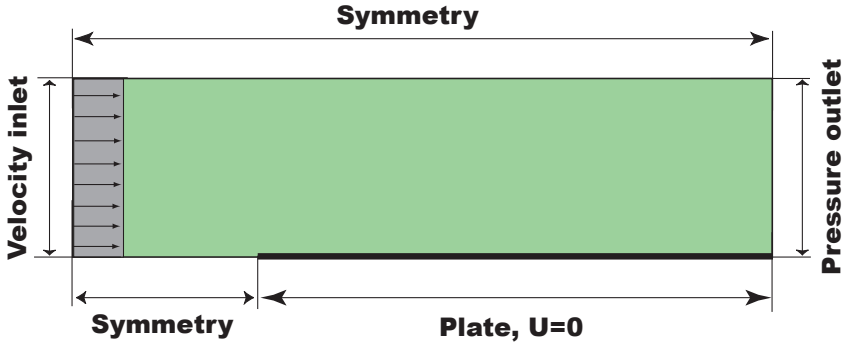

Figure 7.23: Turbulent plate computional domain

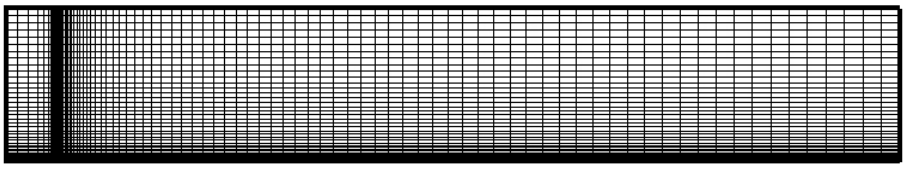

Figure 7.24: Turbulent plate mesh 110x80 cells

At first we will take a look at friction coefficient comparison. Equations (7.15) show experimental correlation of various measurements. When laminar case is computed, c_f after *Blasius* holds, when the flow becomes turbulent the relation after *White* takes hold.

$$\text{Blasius:} \quad c_f = \frac{0.664}{Re_x^{\frac{1}{2}}}, \quad \text{White:} \quad c_f = \frac{0.445}{ln^2(0.06 \cdot Re_x)} \tag{7.15}$$

where:

$$Re_x = \frac{\rho_\infty U_\infty x}{\mu_\infty} \tag{7.16}$$

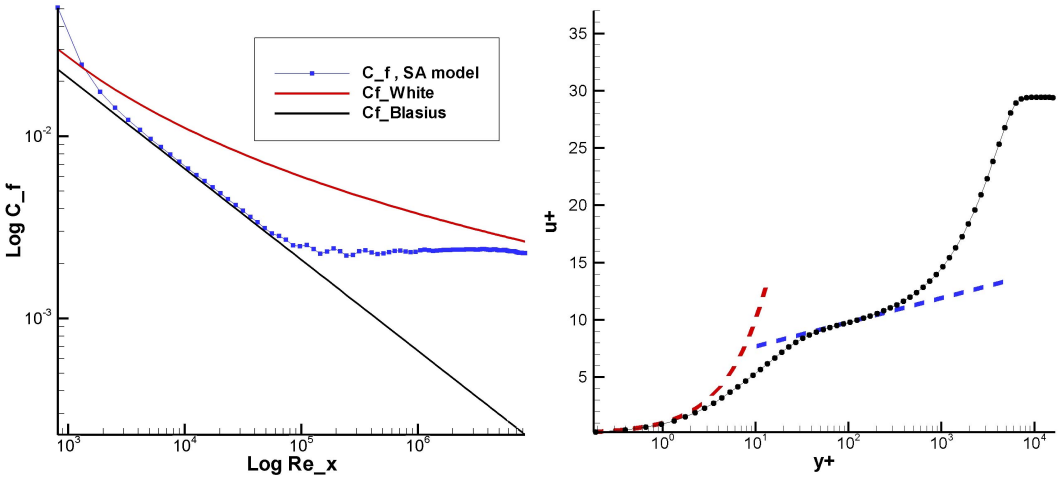

(a) Comparison of friction coefficients

(b) Turbulent boundary layer, SA model

Figure 7.25: Friction coefficients comparison and turbulent boundary layer at the end of the plate

The first figure (a) shows friction coefficient of Spalart-Allmaras model compared with empirically gained correlations.

The second figure (b) shows developed boundary layer at the end of the plate, according to figure 4.1.

7.6.2 C_8 : Turbulent flow in the channel with sudden expansion

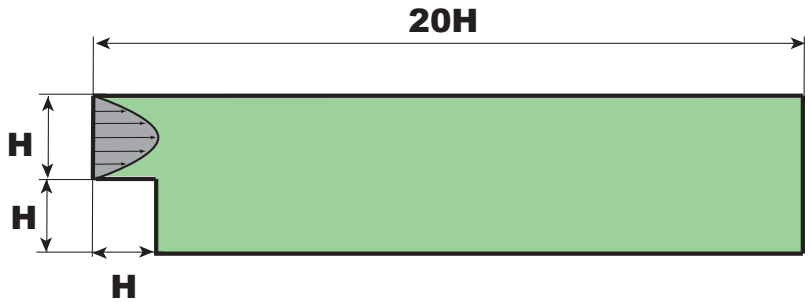

Figure 7.26: Geometry of channel

The geometry of the tested channel shows figure 7.26. This case was experimentally measured by *Armaly* [26]. The mesh used for the case is 100x100 cells. The main characteristics of the case flow are placements of recirculation zones. The flow regime is laminar up to the Reynolds number of 1200 and becomes fully turbulent after overrunning[6] Re=6600. Following figure shows coordinates of recirculation zones:

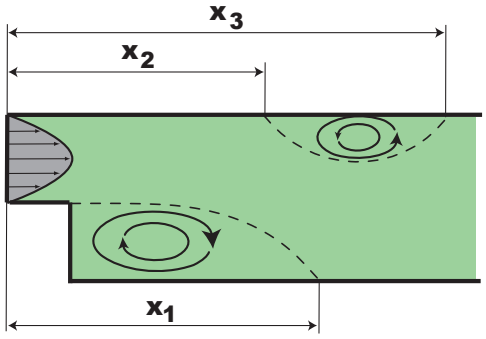

Figure 7.27: Coordinates of recirculation zones

Here the computational domain consists of two parts that have to be connected, as shows the following figure of the mesh:

[6] Armaly [26]

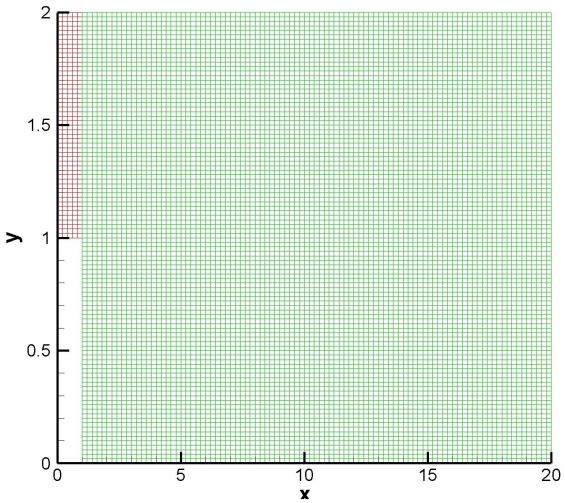

Figure 7.28: The mesh of the test case, 100x100 cells

At first, we made solution for laminar conditions, Re=667:

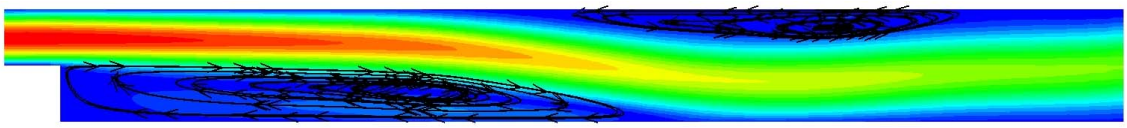

Figure 7.29: Laminar case, Velocity magnitude, Re = 667

Figure 7.29 shows velocity magnitude for laminar case (Re = 667). Here we obtained following results: $x_1 = 11.60$, $x_2 = 9.80$, $x_3 = 17,20$ with agreement with [10].

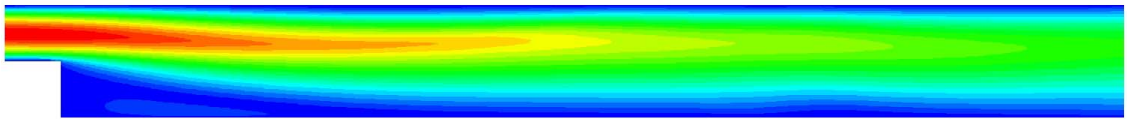

Figure 7.30: Turbulent case, Velocity magnitude, Re = 8000, SA model

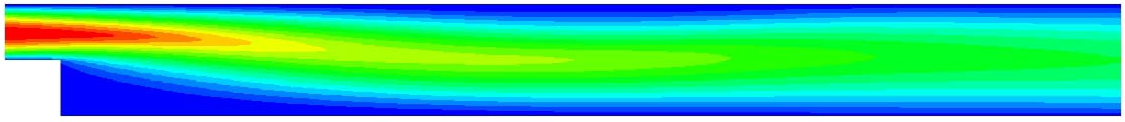

Figure 7.31: Turbulent case, Velocity magnitude, Re = 40000, SA model

For the turbulent cases the recirculation zone at the upper wall completely disappears $x_2 = x_3$. Armaly's measurements gives the length of the recirculation zone at the bottom wall $x_1 = 8.0$.

Figure 7.30 shows velocity magnitude for the turbulent case (Re = 8000). The length of recirculation zone at the bottom wall is $x_1 = 7.20$.

Figure 7.31 shows velocity magnitude for another turbulent case (Re = 40000), here, the length of recirculation zone at the bottom wall is $x_1 = 7.52$ and confirms that x_1 is not[7] depending on Reynolds number in turbulent cases.

[7] e.g. Armaly [26]

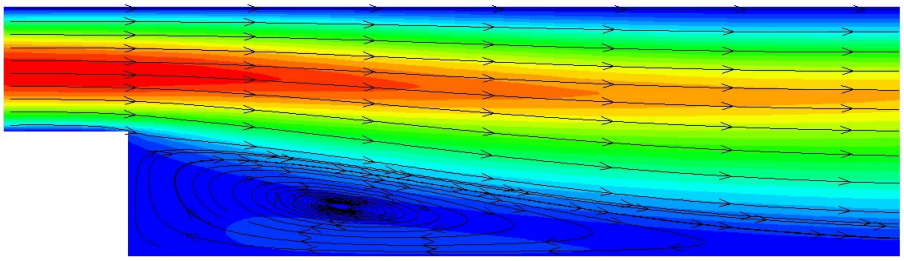

Figure 7.32: Turbulent case, Detail of recirculation zone, Re = 8000, SA model

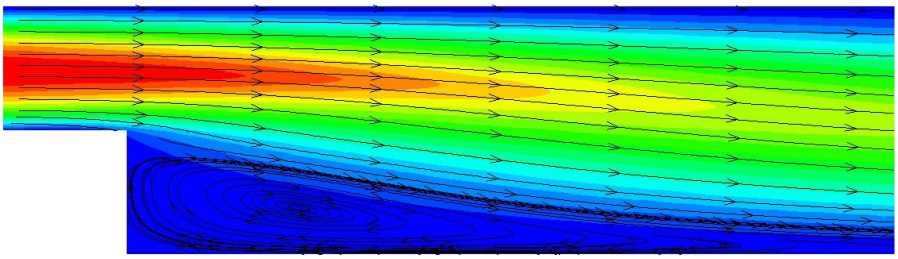

Figure 7.33: Turbulent case, Detail of recirculation zone, Re = 40000, SA model

Figures 7.32 and 7.33 show detail of stream-traces of both turbulent test cases.

7.6.3 C_9 : Turbulent flow over a polynomial hill

This test case was measured by Almeida [27] and now data sets are available in the *ERCOFTAC*'s database [29]. The single hill is defined by an analytical expression: $y = \frac{H}{1+(\frac{x}{H})^4}$, where H is height of the hill. One of the main characteristics is the length of the recirculation zone behind the hill. The geometry of the channel is shown in figure 7.34. The channel diameter is $D = 170mm$, the height of the channel is $H = 28mm$ (16% of diameter). Characteristic lengths are: $L1 = 300mm$, $L2 = 490mm$, $L3 = 790mm$. The mean velocity is $U_0 = 2,147m/s$ and water viscosity $\mu = 1.10^{-3}Pa.s$ leading to Reynolds number $Re = 6.10^4$. The inlet velocity is of profile according to developed laminar flow (equation (7.13)).

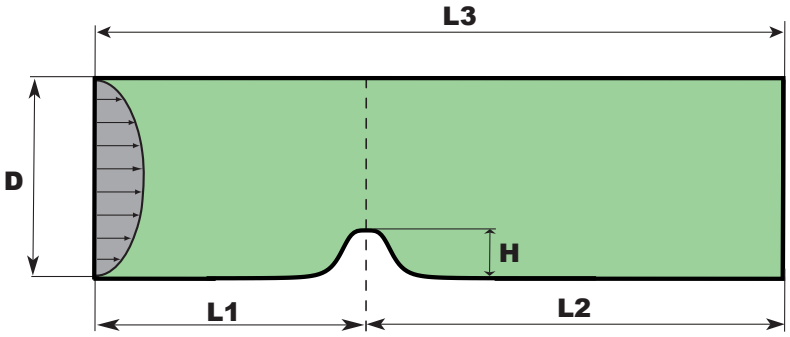

Figure 7.34: Geometry of the channel

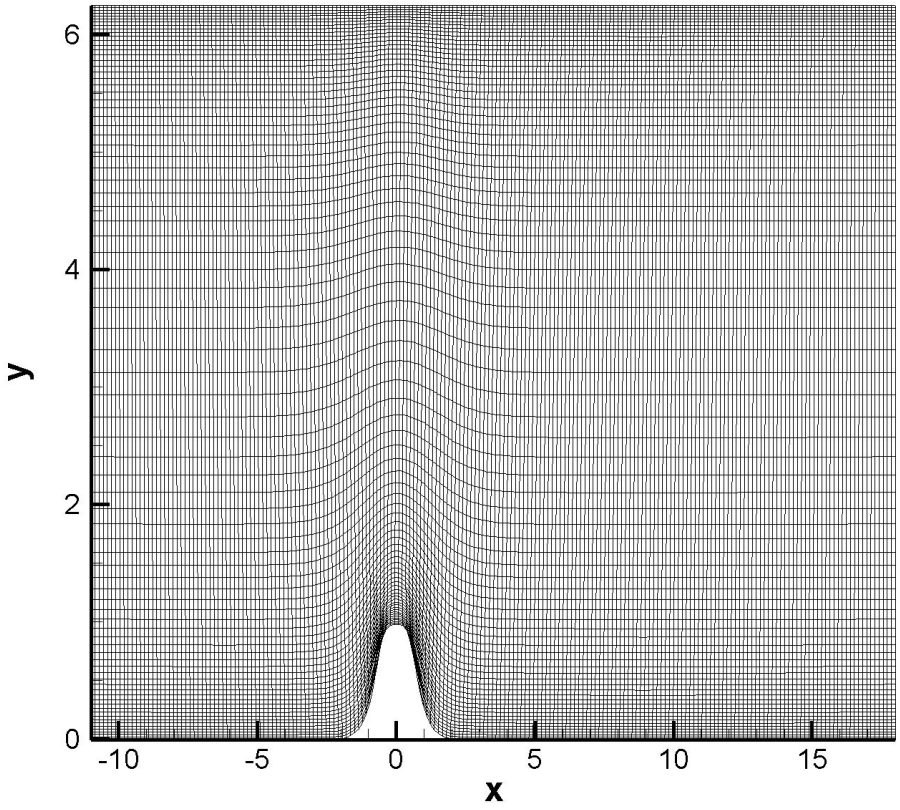

Figure 7.35: The mesh for the channel, 200x80 cells

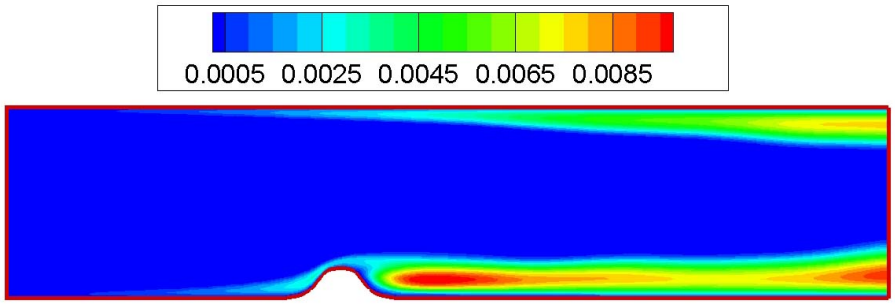

Figure 7.36: Modified eddy viscosity ($\tilde{\nu}$) magnitude, SA model

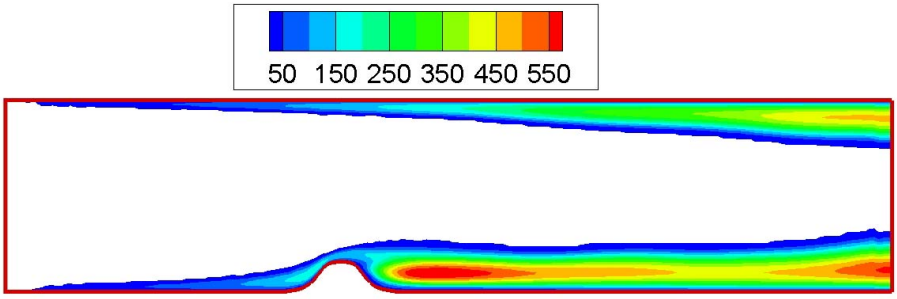

Figure 7.37: Turbulent Reynolds number (Re_T) magnitude, SA model

The figure 7.36 shows modified eddy viscosity ($\tilde{\nu}$) magnitude from Spalart-Allmaras model. The figure 7.37 shows turbulent Reynolds number (Re_T) magnitude, here the cut off color is set on $Re_T \leq 1$. The both above figures look similar, but it is clear from definition.

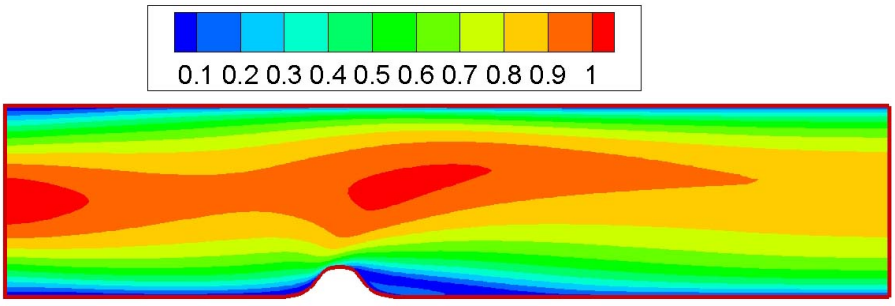

Figure 7.38: Velocity magnitude, SA model

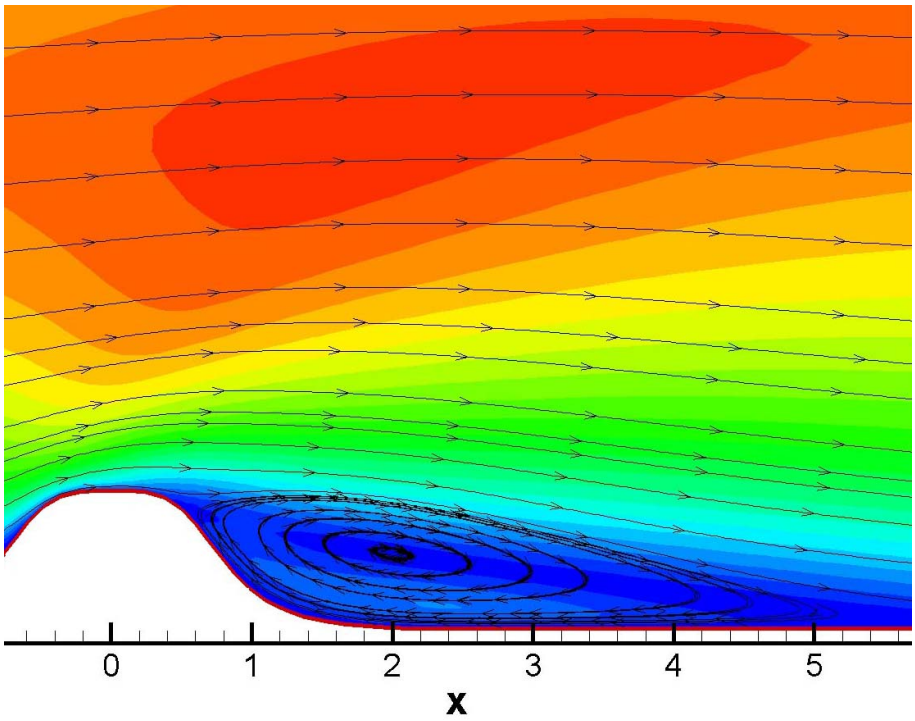

Figure 7.39: Recirculation zone behind the hill, SA model

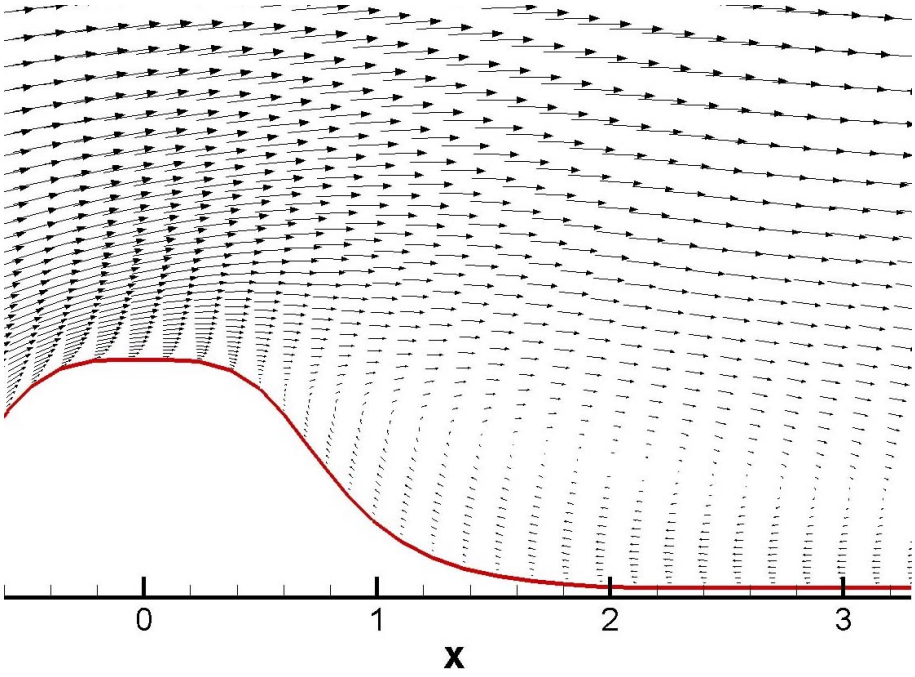

Figure 7.40: Velocity vector field detail, SA model

Figure 7.38 shows velocity magnitude. Figure 7.39 shows the detail of the recirculation zone that appears behind the hill. We have obtained the length of the recirculation zone $L = 5.2H$. Almeida's experiment gives the length of the zone $L = 4.4H$. Ivo Sládek [28] obtained: $L = 4.3H$ (Baldwin-Lomax model) and $L = 3.3H$ ($k - \epsilon$ model) in the same test case. Figure 7.40 shows the detail of velocity vector field behind the hill.

Chapter 8

Conclusion & Remarks

The work was written with afford to be understandable, even if a numerical solution of fluid flow is relatively complicated phenomenon. We have showed, that over a number of simplifications, the introduced model's prediction gives good agreement with experiment or analytical solution.

The presented work has demonstrated:

- Physical basics of solving problems of flow of incompressible viscous fluid and Newtonian, non-Newtonian and turbulent type of flow.
- The way of numerical solution with the help of the Finite Volume Method.
  The first method, we presented (MacCormack scheme with Von Neumann - Richtmayer artificial viscosity), appears to be applicable method, that can be relatively easy implemented. Its advantage is ability to be widely controlled by artificial coefficients.
  The second method, we presented (Causon's Modified TVD MacCormack scheme), is more modern and more accurate method. But can't be controlled and calibrated too much as the previous one.
- The comparison of non-Newtonian viscosity models. All the implemented non-Newtonian viscosity models give approximately identical results and show good applicability.
- The difference between Newtonian and non-Newtonian type of flow. We have shown the differences between pressure distribution and velocity distribution in both cases. These comparisons prove that non-Newtonian behavior of fluid shouldn't be left out if apparently exists.
- Application of the Spalart-Allmaras turbulence model on three typical test cases. SA model showed out to be reliable and widely applicable turbulence model.
- Numerical results' agreement with analytical solutions and renowned measurements.

This work is final result of nearly three years of the studies of The Mathematical Modelling in Technics at The Faculty of Mechanical Engineering at The Czech Technical University.

The solver for numerical solution was completely developed by author in the programming language *C++*. Author estimates the time spent on this project at over 2000 hours of the work (mostly tuning of the program source code) and about 1000 hours of computational time (processor: Intel Pentium 1.4 GHz).

All the presented results are displayed in *Tecplot 10.0*. All the meshes (except the both flat plates meshes) we have generated partly in *C++*, partly in *Tecplot 10.0*. The pictures are made in *Adobe Illustrator CE 10.0*. The work itself was typeset by TEX in *WinEdt 5*.

After vindication of this work at school final examination author is ready to release to anyone the source code of the solver or any part of this project on request. Eventual questions or reminders please send to: *Lubos.Pirkl@seznam.cz*.

■

References

[1] Dvořák R., Kozel K.: Matematické modelovaní v aerodynamice. Vydavatelství ČVUT, 1996.

[2] Bodnár T., Numerical Simulation of Flows and Pollution Dispersion in Atmospheric Boundary Layer. CTU Thesis, 2003

[3] Wilcox D.C. Turbulence Modeling for CFD, DCW Industries

[4] Fürst J., Numerické řešení transonického proudění užitím TVD a ENO schémat, Disertační práce, 2000

[5] LeVeque R. J., Numerical Methods for Conservation Laws. Birkhauser Verlag, 1990

[6] Beneš L., Numerické řešení proudění v mezní vrstvě atmosféry. Thesis 2000

[7] Hirsh C., Numerical Computation of INTERNAL and EXTERNAL FLOWS Volume 2 Computational Methods for Inviscit and Viscous Flows, WILEY, 1990

[8] Fořt J., Fürst J., Kozel K., Louda P., Numerické metody řešení problému proudení I., II., III. Vydavatelství CVUT, 2001 - 2004.

[9] Šesták J., Rieger F., Přenos hybnosti, tepla a hmoty, Vydavatelství ČVUT, 1998

[10] Kozel K., Louda P., Bodnár T., Beneš L., Sládek I., Numerická simulace proudění II

[11] Petkova S., Hossain A., Naser J., Palombo E., CFD Modelling of blood in portal Vein Hypertension with and Without Thrombosis, CSIRO, Melbourne, Australia,2003.

[12] Cheng D. C-H., Heywood N.I., Flow in Pipes, Physical Technology, Northern Ireland, 1984.

[13] Hackley H.A., Ferraris C.F., The Use of Nomenclature in Dispersion Science and Technology, National Institute of Standards and Technology 2001

[14] Schramm G., A Practical Approach to Rheology and Rheometry, Gebrueder HAAKE Gmbh, Karlsruhe,1998

[15] Hughes W.F., Brighton J.A., Fluid Dynamics, Schaum 1991

[16] Příhoda J., Louda P., Matematické modelování turbulentního prodění,Vydavatelství ČVUT, 2007.

[17] Cho, Y.I., Kensey, K.R., Effects of Non-Newtonian Viscosity of Blood on Flows in Diseased Arterial Vessel, Part 1: Steady Flows, vol.28 (1991), pp. 41-262.

[18] Krishna Kumar Yeleswarapu, Evaluation of Continuum Models for Characterizing the Constitutive Behavior of Blood, University of Pittsburgh, 1996.

[19] Pirkl L., Bodnár T., Numerical Simulation of non-Newtonian Fluid Flow Using Generalised Nevier-Stokes Models, Colloquium FUID DYNAMICS 2006, Institute of Thermomechanics AS CR, Prague October 25-27, 2006

[20] Pedrizzetti G., Perktold K., Cardiovascular Fluid Mechanics, Courses and Lectures - No.446

[21] Baldwin B. S., Lomax H., Thin Layer Approximation and Algebraic Model for Separated Turbulent Flows, AIAA Paper 78-257, (1978).

[22] Rostand P., Algebraic Turbulence models for the Computation of Two-dimensional High Speed Flows Using Unstructured Grids, NASA CR-181741, (1988).

[23] Fujisawa N., Rodi W., Schönung B., Calculation of Transitional Boundary Layers with a Two-Layer Model of Turbolence, Institute for Hydromechanics, University of Karlsruhe, (1990).

[24] Spalart P.R., Allmaras S.R., A One-equational Turbulence Model for Aerodynamic Flows, AIAA, Paper 92-0439, (1992).

[25] Acheson D.J., Elementary Fluid Dynamics, Oxford Applied Matematics and Computing Science Series, (1990).

[26] Armaly B.F., Durst F., Pereira J. C. F., Schönung B., Experimental and theoretical investigation of backward-facing step flow. J. Fluid Mech., Sv. 127: (1983)

[27] Almeida, G.P., Durao, D.F.G. ,Heitor, M.V. Wake flows behind two dimensional model hills. Exp. Thermal and Fluid Science, 7, p.87, (1992).

[28] Sládek I., Mathematical Modelling and Numerical Solution of Some 2D and 3D Cases of Atmospheric Boundary Layer flow, The Czech Technical University, Prague, 2004.

[29] http://www.ercoftac.org/ , European Research Community On Flow, Turbulence And Combustion, internet pages.

[30] http://www.britannica.com/ , Encyclopedia Britannica, Inc., internet pages.

[31] http://en.wikipedia.org/ , internet pages.

[32] http://www.cfd-online.com/ , internet pages.

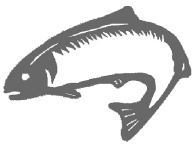

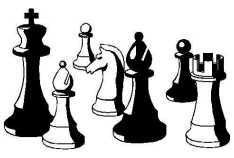


SK SLAVIA PRAHA
FOTBAL